# Isolation of [Ru(IPr)$_2$(CO)H]$^+$ (IPr = 1,3-Bis(2,6-diisopropylphenyl)imidazol-2-ylidene) and Reactivity toward E−H (E = H, B) Bonds

Ian M. Riddlestone,[†] David McKay,[‡,⊥] Matthias J. Gutmann,[§] Stuart A. Macgregor,[*,‡] Mary F. Mahon,[*,†] Hazel A. Sparkes,[*,∥] and Michael K. Whittlesey[*,†]

[†]Department of Chemistry, University of Bath, Claverton Down, Bath BA2 7AY, U.K.
[‡]Institute of Chemical Sciences, Heriot-Watt University, Edinburgh EH14 4AS, U.K.
[§]ISIS Facility, STFC-Rutherford Appleton Laboratory, Didcot OX11 OQX, U.K.
[∥]School of Chemistry, University of Bristol, Cantock's Close, Bristol BS8 1TS, U.K.

Ⓢ *Supporting Information*

**ABSTRACT:** Halide abstraction from the ruthenium N-heterocyclic carbene complex Ru(IPr)$_2$(CO)HCl (IPr = 1,3-bis(2,6-diisopropylphenyl)imidazol-2-ylidene) with NaBAr$_4^F$ (BAr$_4^F$ = B{C$_6$H$_3$(3,5-CF$_3$)$_2$}$_4$) gave the salt [Ru(IPr)$_2$(CO)-H]BAr$_4^F$ (**2**), which was shown through a combined X-ray/neutron structure refinement and quantum theory of atoms in molecules (QTAIM) study to contain a bifurcated Ru···$\eta^3$-H$_2$C $\xi$-agostic interaction involving one $^i$Pr substituent of the IPr



Combined Synthetic/X-ray/Neutron/QTAIM Studies

ligand. This system complements the previously reported [Ru(IMes)$_2$(CO)H]$^+$ cation (IMes =1,3-bis(2,4,6-trimethylphenyl)-imidazol-2-ylidene), where a non-agostic form is favored. Treatment of **2** with CO, H$_2$, and the amine−boranes H$_3$B·NR$_2$H (R = Me, H) gave [Ru(IPr)$_2$(CO)$_3$H]BAr$_4^F$ (**3**), [Ru(IPr)$_2$(CO)($\eta^2$-H$_2$)H]BAr$_4^F$ (**4**), and [Ru(IPr)$_2$(CO)($\kappa^2$-H$_2$BH·NR$_2$H)H]BAr$_4^F$ (R = Me, **5**; R = H, **6**), respectively. Heating **5** in the presence of Me$_3$SiCH=CH$_2$ led to alkene hydroboration and formation of the C−H activated product [Ru(IPr)(IPr)$'$(CO)]BAr$_4^F$ (**7**). X-ray characterization of **3** and **5**−**7** was complemented by DFT calculations, and the mechanism of H$_2$/H exchange in **4** was also elucidated. Treatment of **2** with HBcat resulted in Ru−H abstraction to form the boryl complex [Ru(IPr)$_2$(CO)(Bcat)] BAr$_4^F$ (**8**), which proved to be competent in the catalytic hydroboration of 1-hexene. In **8**, a combined X-ray/neutron structure refinement and QTAIM analysis suggested the presence of a single Ru···$\eta^2$-HC $\xi$-agostic interaction.
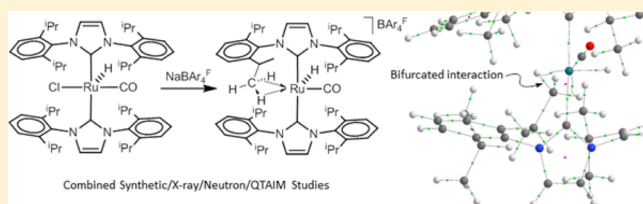
## ■ INTRODUCTION

The preparation of coordinatively unsaturated transition-metal complexes is a widespread pursuit for practitioners of organometallic chemistry with an eye to developing new or improved reactivity of organic substrates. In the case of ruthenium, efforts to generate low-coordinate Ru(0) species date from the mid 1960s with Chatt's attempted synthesis of the 16-electron chelating phosphine complex Ru(dmpe)$_2$ (dmpe = 1,2-bis(dimethylphosphino)ethane),[1] which was employed in some of the earliest attempts to bring about intra- and intermolecular C−H bond activation.[2] It is now known that this species is far too reactive to exist as anything other than a transient intermediate that can only be detected at very low temperature in inert-gas matrices or in solution on very short, pico- to nanosecond time scales.[3] However, some 30 years after Chatt's studies, Caulton[4] and Werner[5] demonstrated that Ru$^0$L$_4$ species could indeed be isolated (and even structurally characterized) given the appropriate choice of L ligands; namely, bulky phosphines in combination with $\pi$-accepting carbonyl or nitrosyl groups.

Arguably, the preparation of four-coordinate Ru$^{II}$L$_4$ species is an even greater synthetic challenge, on the grounds of their greater electron deficiency: i.e., a 14-electron count. Such species are therefore, unsurprisingly, rare (Chart 1). The chelate complexes Ru(PNP)Cl (**A**) and Ru(PO)$_2$ (**B**) adopt triplet ground states, which appear to be enough to reduce their Lewis acid character.[6] Upon changing N(SiMe$_2$CH$_2$P$^t$Bu$_2$)$_2$ for N(CH$_2$CH$_2$P$^t$Bu$_2$)$_2$, Ru(PNP)Cl (**C**) displays a square-planar structure and a singlet ground state due to the combination of

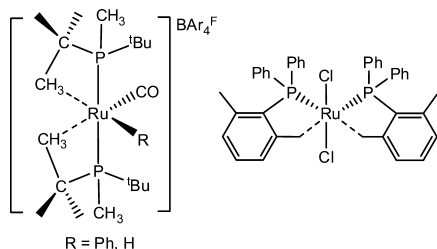**Chart 1**
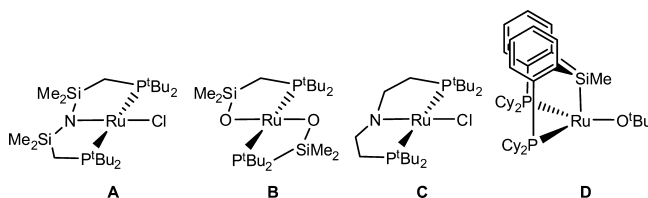
high ligand sterics and strong N→Ru π-donation.[7] This same combination of steric and electronic donor properties also appears to help rationalize the stability of (Cy-PSiP)RuO^tBu (**D**).[8] In other species, such as [Ru(P^tBu_2Me)_2(CO)R]^+ (R = Ph, H)[9−11] and Ru(PPh_2{2,6-C_6Me_2H_3})_2Cl_2 (Chart 2),[12]

**Chart 2**



stabilization benefits from the presence of Ru···H−C agostic interactions to afford complexes which react as latent 14-electron species.[12−15] Thus, the X-ray structures of both [Ru(P^tBu_2Me)_2(CO)Ph]^+ and [Ru(P^tBu_2Me)_2(CO)H]^+ exhibit sawhorse configurations, in which both of the remaining vacant coordination sites at ruthenium are occupied by agostic interactions from the phosphine ^tBu groups. In the case of Ru(PPh_2{2,6-C_6Me_2H_3})_2Cl_2, neutron diffraction reveals an even more unusual stabilizing effect involving two sets of bifurcated agostic Ru···η^3-H_2C interactions.[16]

Our interest in Ru^IIL_4 species was raised by the report of Gunnoe and co-workers from a number of years ago which identified the cationic N-heterocyclic carbene (NHC) derivative [Ru(IMes)_2(CO)H]^+ (**1**, Scheme 1; IMes = 1,3-bis(2,4,6-

**Scheme 1. Gunnoe's Reported Synthesis of [Ru(IMes)_2(CO)H]BAr_4^F (1)[17]**
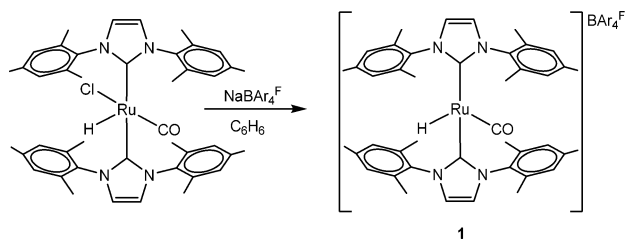


trimethylphenyl)imidazol-2-ylidene) as a true four-coordinate Ru(II) species devoid of any agostic stabilization.[17] All attempts to isolate **1** for structural verification proved unsuccessful, unfortunately, and hence characterization was based upon DFT calculations and chemical trapping experiments. Given that variations of NHC N substituents can often be used to bring about significant changes in the structure/reactivity of coordinatively unsaturated M(NHC)_x complexes,[18] we have employed the bulkier IPr (1,3-bis(2,6-diisopropylphenyl)-imidazol-2-ylidene) ligand for the generation of [Ru-(IPr)_2(CO)H]^+ (**2**). Structural methods (neutron/X-ray diffraction) and DFT calculations have shown that **2** is stabilized by a symmetric bifurcated Ru···η^3-H_2C ξ-agostic interaction involving an ^iPr methyl group. In solution, **2** undergoes facile coordination of neutral donor ligands (CO, H_3B·NR_2H (R = Me, H)) and B−H activation of a borane as well as intramolecular C−H activation of an IPr ligand.

## RESULTS AND DISCUSSION

### Synthesis and Characterization of [Ru(IPr)_2(CO)H]^+.
The BAr_4^F (B{C_6H_3(3,5-CF_3)_2}_4) salt of [Ru(IPr)_2(CO)H]^+ (**2**) was isolated in high yield (80%) as a highly air and moisture sensitive dark orange solid upon chloride abstraction from Ru(IPr)_2(CO)HCl[19] with NaBAr_4^F in C_6H_5F at room temperature over 12 h (Scheme 2).

**Scheme 2. Synthesis of the BAr_4^F Salt of [Ru(IPr)_2(CO)H]^+ (2)[a]**
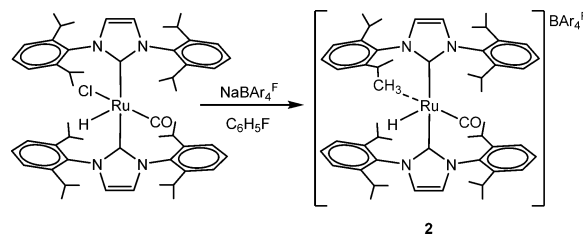


[a]Both here and in later graphics, the dotted contact between Ru and an ^iPr methyl group represents the likelihood that some H_3C···Ru agostic interaction is retained in solution.

An X-ray structure determination on crystals of the compound isolated from fluorobenzene/hexane revealed two components, which in each case showed the presence of an ξ-agostic interaction between the metal and one of the ^iPr methyl substituents. This agostic C−H interaction lies trans to the CO group, with the hydride ligand disordered over the remaining two coordination sites, trans to each other, in the equatorial plane. To examine this in more detail, we combined neutron diffraction data with those from X-ray measurements in a joint refinement. The cation of the major (55%) component (**2a**) is shown in Figure 1. Interestingly, the presence of two similar,
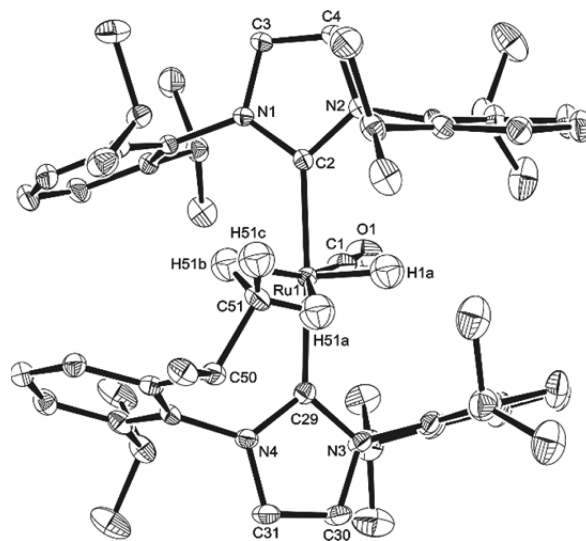


**Figure 1.** Combined neutron/X-ray structure of the cation in [Ru(IPr)_2(CO)H]BAr_4^F (major component, **2a**). Ellipsoids are shown at the 30% probability level with all hydrogen atoms (except Ru−H and those on the agostic methyl group) removed for clarity. Selected bond lengths (Å) and angles (deg): Ru(1)−C(2) 2.102(3), Ru(1)−C(29) 2.091(4), Ru(1)−C(1) 1.796(4), Ru(1)···C(51) 2.589(3), Ru(1)···H(51A) 2.21(2), Ru(1)···H(51B) 2.14(2), C(51)−H(51A) 1.09(2), C(51)−H(51B) 1.13(2), C(1)−O(1) 1.160(5); C(2)−Ru(1)−C(29) 176.51(13).

short Ru⋯H−C contacts (Ru(1)⋯H(51A) 2.21(2) Å, Ru(1)⋯
H(51B) 2.14(2) Å, Ru(1)⋯H(51c) 3.27(2) Å)) supported the
presence of a bifurcated Ru⋯$\eta^3$-H$_2$C agostic interaction far
more symmetric in nature than that seen in Ru(PPh$_2${2,6-
C$_6$Me$_2$H$_3$})$_2$Cl$_2$, where the Ru⋯H−C distances ranged from
2.113(10) to 2.507(11) Å.[16] Conejero has reported that the
C−H activated NHC complex [Pt(IPr)(IPr)′]SbF$_6$[20] exhibits a
single ξ-agostic interaction to the nonactivated IPr ligand with
Pt⋯H and Pt⋯C distances of 2.017(6) and 2.8760(1) Å,
respectively, and a Pt⋯H−C angle of 145°. In **2a**, the Ru(1)⋯
C(51) distance is considerably shorter (2.589(3) Å), with Ru⋯
H−C angles (Ru(1)⋯H(51A)−C(51)/Ru(1)⋯H(51B)−
C(51)) of 97.4(11) and 100.2(11)°.

Further insight into the nature of the agostic interaction in **2a**
was obtained from a quantum theory of atoms in molecules
(QTAIM)[21] study, where the experimental structure of **2a** was
used directly in the QTAIM analysis (Figure 2). This highlights
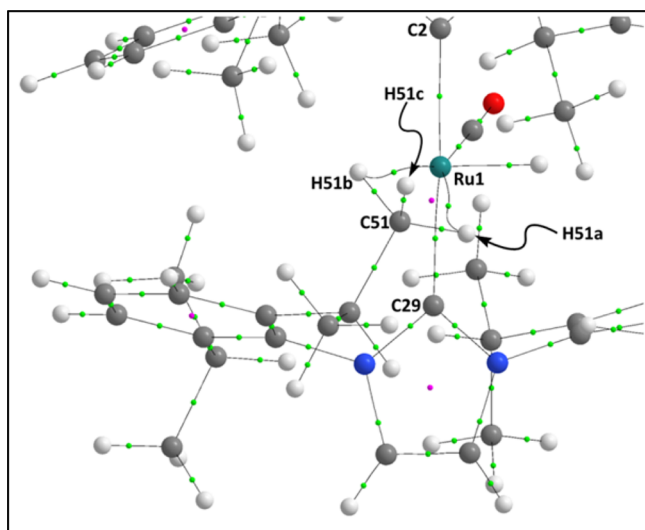


**Figure 2.** QTAIM molecular graph of the cation of the major
component **2a**, focusing on the Ru1⋯H51a/H51b interactions.
Calculations were based on the experimental X-ray/neutron structure
and used the BP86 functional. Bond critical points (BCPs) and ring
critical points (RCPs) are shown as green and magenta spheres,
respectively. Selected $\rho(r)$ values (au): BCPs, Ru1⋯H51b 0.038 and
Ru1⋯H51a 0.033; RCP, Ru1⋯H51b−C51-H51a 0.033. See the
Supporting Information for full QTAIM metrics.

curved bond paths associated with both the Ru⋯H51a and
Ru1⋯H51b contacts, indicative of bonding interactions and so
consistent with a bifurcated Ru⋯$\eta^3$-H$_2$C structure. This is
further confirmed by the presence of a ring critical point (RCP)
enclosed by the {Ru1⋯H51b−C51−H51a} unit. The com-
puted BCP electron densities, $\rho(r)$, are relatively low at ca.
0.035 au and suggest that, despite the short Ru⋯H51a/H51b
and Ru⋯C51 distances, the resultant agostic interactions are
relatively weak.[22]

**2b**, the cation within the second component present in the
combined neutron/X-ray structure of **2**,[23] shows a geometry
around Ru1 very similar to that of **2a**, with Ru⋯H51a and
Ru1⋯H51b contacts of 2.23(2) and 2.16(2) Å, respectively,
and a short Ru−C(51) contact of 2.590(3) Å. QTAIM
calculations also confirm a bifurcated structure. In addition, a
third Ru⋯$\eta^2$-HC contact of 2.44(2) Å to an $^i$Pr substituent
located trans to the hydride ligand is seen, although the

associated BCP has a low $\rho(r)$ value of only 0.012 au (see
computational details in the Supporting Information).

We were unable to affirm that the Ru⋯H−C interactions
persisted in solution, as the four doublets and two septets of the
$^i$Pr groups observed by $^1$H NMR spectroscopy at room
temperature simply broadened rather than separated upon
cooling to 194 K.[24] Low-temperature (200 K) $^{13}$C{$^1$H} and $^1$H-
coupled $^{13}$C NMR spectra showed neither any low-frequency-
shifted methyl resonance nor any reduced $^1J_{CH}$ coupling
constant (Supporting Information). The low frequency of the
hydride chemical shift ($\delta$ −23.9 at 298 K) was similar to those
of both Ru(IPr)$_2$(CO)HCl and **1** as a result of the vacant trans
coordination site. Notably, NMR measurements of **2** (including
$^{13}$C spectra accumulated overnight) could be recorded in
CD$_2$Cl$_2$ and gave spectra nearly identical with those recorded in
fluorobenzene, revealing that, unlike [Ru(P$^t$Bu$_2$Me)$_2$(CO)H]$^+$,
there was no binding of dichloromethane.[11,25] Presumably, the
Lewis acidity of **2** is lowered by the presence of the two
strongly σ donating NHC ligands which, in combination with
their steric bulk, disfavor interaction with a poor base such as
CH$_2$Cl$_2$. A small amount of decomposition of **2** was evident by
NMR spectroscopy (only after several days) in chlorinated
solvents or upon warming to 343 K in C$_6$H$_5$F, although there
was no evidence to suggest that this involved dehydrogenation
of the carbene N substituent as seen for [Ir(IPr)$_2$H$_2$]$^+$.[26]

**Experimental and Computational Comparison of
[Ru(IPr)$_2$(CO)H]$^+$ and [Ru(IMes)$_2$(CO)H]$^+$.** In Gunnoe's
attempts to prepare **1**, benzene was used as the solvent for
the attempted NaBAr$_4$$^F$ abstraction. Upon turning to C$_6$H$_5$F,
we found no discernible change in color of the solution but did
observe a change in the hydride region of the proton NMR
spectrum, the signal for **1** at $\delta$ −25.4 being replaced by a new
resonance at $\delta$ −29.9 within the time of mixing Ru-
(IMes)$_2$(CO)HCl and NaBAr$_4$$^F$. The species responsible for
this new signal proved to be stable for at least 48 h.
Comparison with Aldridge's studies on NaBAr$_4$$^F$ abstraction
of chloride from M(IMes)$_2$H$_2$Cl (M = Rh, Ir),[26] in particular
the shift of the hydride signal to lower frequency, led us to
propose the formation of the sodium inclusion complex
[Ru(IMes)$_2$(CO)HCl(Na)]BAr$_4$$^F$, in which the sodium cation
is intercalated between the mesityl rings of the NHC. All efforts
to isolate this species with the aim of confirming this
assignment were unsuccessful. Similar behavior was found
upon re-examining the Ru(IPr)$_2$(CO)HCl/NaBAr$_4$$^F$ reaction. A
$^1$H NMR spectrum recorded 15 min after mixing the reagents
showed loss of the starting Ru−H resonance ($\delta$ −24.5) and
formation of new signals at both higher ($\delta$ −23.9) and lower ($\delta$
−28.2) frequencies, assigned to **2** and [Ru(IPr)$_2$(CO)HCl-
(Na)]BAr$_4$$^F$, respectively. After 48 h, only the hydride signal for
**2** remained, consistent with the inclusion complex being an
intermediate on the pathway to full metathesis. Quite why the
IMes derivative is so much longer lived than the IPr derivative
is unclear. Different behavior was also apparent using
[Et$_3$Si(toluene)]BAr$_4$$^F$ for halide abstraction instead of
NaBAr$_4$$^F$. Ru(IPr)$_2$(CO)HCl was now converted instantly
and cleanly through to **2**, whereas with Ru(IMes)$_2$(CO)HCl,
there was no clear evidence for the formation of a hydride-
containing product at all.

As a structural comparison of **1** and **2** was not possible
experimentally, DFT calculations were employed to probe the
differences between these two systems. Geometries were now
fully optimized with the BP86 functional: for **2a,b** input

geometries were based on the X-ray/neutron structures, and these structures were adapted to produce input geometries for their IMes analogues **1a,b**. The reported free energies include corrections for dispersion (D3 parameter set) and $C_6H_5F$ solution (PCM approach). For $[Ru(IPr)_2(CO)H]^+$, the optimized structures of **2a,b** gave good agreement in the heavy-atom positions but showed rotation around the C(50)−C(51) bond such that the bifurcated Ru⋯$\eta^3$-$H_2C$ agostic interactions were replaced by a single Ru⋯$\eta^2$-H(51a)−C(51) agostic interaction (**2a**, Ru(1)⋯H(51a) = 2.01 Å, Ru(1)⋯H(51b) = 2.54 Å; **2b**, Ru(2)⋯H(51a) = 1.96 Å, Ru(2)⋯H(51b) = 2.63 Å). In addition, for **2b**, the short Ru⋯H contact trans to hydride noted experimentally shortens to 2.14 Å in the calculated structure, which therefore features two single Ru⋯$\eta^2$-H−C agostic interactions, one trans to each of the CO and H ligands. In the course of these studies an alternative conformer bereft of any agostic interaction (**2c**) was also located in which the closest Ru⋯H contact was 3.87 Å. Of these three forms, **2b** is computed to be the most stable in $C_6H_5F$ solution with **2a,c** respectively 0.8 and 3.0 kcal/mol higher in energy.

Three equivalent structures were also located for $[Ru(IMes)_2(CO)H]^+$, but now the nonagostic form **1c** was the most stable in $C_6H_5F$ solvent (cf. **1a** at +1.8 kcal/mol and **1b** at +2.1 kcal/mol). Although these computed differences are small, the tendency to form agostic interactions is clearly greater in $[Ru(IPr)_2(CO)H]^+$ in comparison to $[Ru(IMes)_2(CO)H]^+$.[27] This reflects the greater ability of the $^iPr$ substituents to interact with the Ru center without undue deformation of the NHC ligand. For example, in **2a** the angle between the plane of the central imidazol-2-ylidene ring and that of the aryl group of the 2,6-$^iPr_2C_6H_3$ substituent engaged in the agostic interaction is 75.3°, whereas the equivalent angle with the mesityl substituent in **1a** is 55.8°.

Further evidence for **2** retaining an agostic interaction in solution comes from the different colors observed for solutions of **1** (brick red)[17] and **2** (orange). TDDFT calculations (CAMB3LYP($C_6H_5F$)//BP86) indicate that the lowest-lying absorption is dominated by a d−d transition between the HOMO and LUMO of the system and show that this is blue-shifted in the presence of an agostic interaction (**1a**, 440 nm; **1b**, 432 nm; **1c**, 477 nm; **2a**, 399 nm; **2b**, 390 nm; **2c**, 486 nm). This reflects the interaction of the C−H bond with the $\{Ru(NHC)_2(CO)H\}^+$ fragment (NHC = IMes, IPr) in the agostic structures **1a,b** and **2a,b**, which has the effect of destabilizing the LUMO. Orbital plots are provided in the Supporting Information.

**Coordination of CO, $H_2$, and B−H Bonds to [Ru-(IPr)$_2$(CO)H]$^+$.** Addition of 1 atm of CO to a fluorobenzene solution of **2** resulted in displacement of the agostic bonding and coordination of two additional CO ligands to yield the 18-electron tricarbonyl compound $[Ru(IPr)_2(CO)_3H]BAr_4^F$ (**3**, Scheme 3). The presence of a high-frequency-shifted ($\delta$ −6.81)

hydride singlet was indicative of the coordinative saturation.[13a] Use of $^{13}CO$ led to signal enhancement of just the two lowest frequencies of the three $^{13}C\{^1H\}$ NMR carbonyl resonances at $\delta$ 173, 190, and 193, consistent with the initial Ru−CO group being inert to substitution. The cis-$^{13}C$-labeled CO ligands (Scheme 3) showed the expected small (4 Hz) $^2J_{CC}$ splitting. Both signals coupled to the Ru−H resonance, to generate a doublet of doublets signal, with $^2J_{HC}$ couplings of 26.1 (trans) and 6.7 Hz (cis).

Of note in the X-ray structure of **3** (Figure 3) were the distortions of the three distinctly nonlinear Ru−C−O bonds.
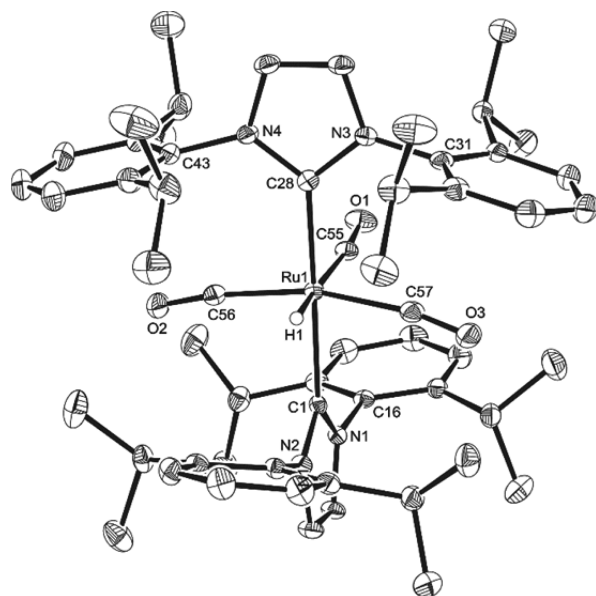


**Figure 3.** Molecular structure of the cation in $[Ru(IPr)_2(CO)_3H]$-$BAr_4^F$ (**3**). Ellipsoids are shown at the 30% probability level with all hydrogen atoms (except Ru−H) removed for clarity. Selected bond lengths (Å) and angles (deg): Ru(1)−C(1) 2.140(2), Ru(1)−C(28) 2.129(3), Ru(1)−C(55) 1.976(3), Ru(1)−C(56) 1.922(3), Ru(1)−C(57) 1.945(3); C(1)−Ru(1)−C(28) 171.64(10), C(55)−Ru(1)−C(56) 91.81(12), C(56)−Ru(1)−C(57) 166.09(12).

The 81° angle between the two mean planes (each containing the atoms of an NHC ring) revealed that the carbene ligands are disposed at the upper limit of a staggered arrangement. Moreover, the three carbonyl ligands about the equatorial girdle of the cation were each seen to lie atop an IPr phenyl ring (C55/O1 above the ring based on C16; C56/O2 above the ring based on C43, and C57/O3 above the ring based on C31). The ensuing steric factors have combined such that the CO ligands are each bent away from the face of the aromatic ring above which each is located. These features are retained in the BP86-optimized structure of **3** but lost in the less congested model species $[Ru(IMe)_2(CO)_3H]^+$ (**3′**, IMe = 1,3-dimethyl-imidazol-2-ylidene), confirming their steric origin (similar deviations from linearity can also arise from electronic effects[4a]). The carbonyl oxygens appear to have borne the maximum brunt of these distortions away from the plane of the proximate aromatic rings (Ru(1)−C(55)−O(1) 171.9(2)°, Ru(1)−C(56)−O(2) 171.6(2), Ru(1)−C(57)−O(3) 169.1(2)) away from the plane of the proximate aromatic ring. These compare to the values of 177.6(5), 176.9(5), and 175.1(5)° found in the cationic phosphine derivative $[Ru-(PPh_3)_2(CO)_3H]^+$.[28] Ultimately, "bowing" of the two trans

**Scheme 3**
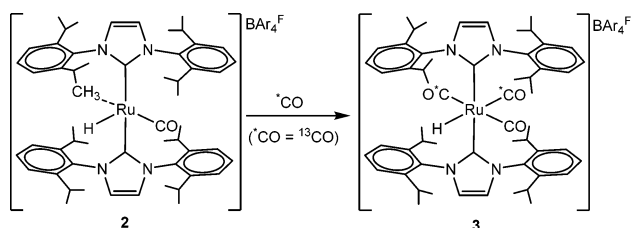
**Scheme 4**
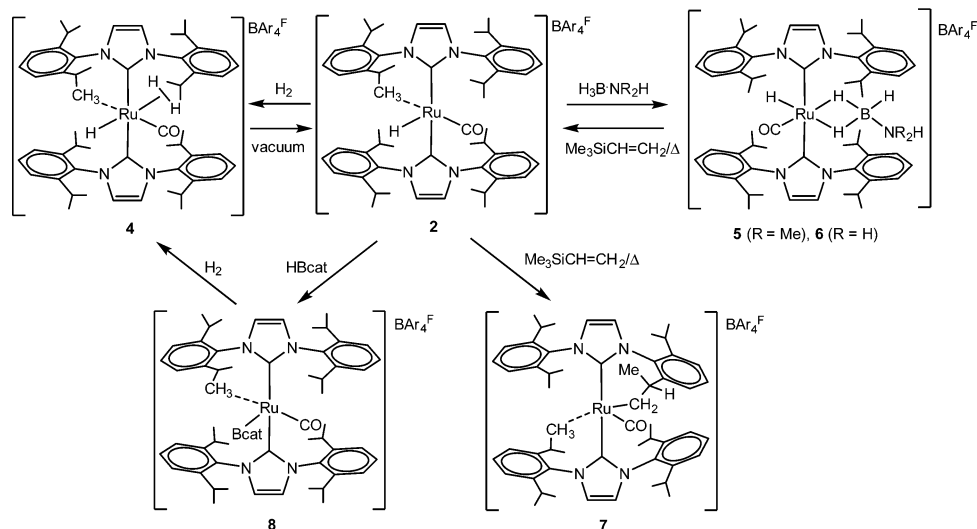


carbonyl groups in **3** is evidenced by the C(56)−Ru(1)−C(57) angle of 166.09(12)°. The trans influence of the hydride ligand manifests itself in the elongation of the Ru(1)−C(55) distance (1.976(3) Å) relative to the other two Ru−CO bond lengths (1.945(3) and 1.922(3) Å).

Introduction of $H_2$ (1 atm) into a $CD_2Cl_2$ solution of **2** brought about an immediate color change from orange to yellow resulting from the formation of the dihydrogen hydride complex $[Ru(IPr)_2(CO)(\eta^2\text{-}H_2)H]BAr_4^F$ (**4**, Scheme 4). At room temperature, this showed a single, broad hydride resonance at $\delta$ −4.95 of relative integral 3, suggestive of rapidly exchanging Ru−H/$(\eta^2\text{-}H_2)$ ligands. Even at 182 K, the exchange could not be frozen out, an observation that is in line with other ruthenium complexes containing a cis arrangement of dihydrogen and hydride ligands.[29,30] Freeze−pump−thaw degassing failed to completely remove the $\eta^2\text{-}H_2$ ligand, and the resonance at $\delta$ −4.95 could still be seen even after 10 degassing cycles.[31] When the solution of **4** was reduced to complete dryness, **2** was regenerated.

DFT calculations were employed to provide structural insight into **4**, and three local minima were again located, two of which feature a single agostic interaction, either trans to CO (**4a**) or H (**4b**), and a third, nonagostic form (**4c**). All three isomers are within 0.9 kcal/mol of each other when computed at the BP86-D3($CH_2Cl_2$) level (Figure 4a). A transition state for Ru−H/$(\eta^2\text{-}H_2)$ exchange, **TS(4b-4b)**, was also located. This process involves H transfer from the original $\eta^2\text{-}H_2$ ligand in **4b** (labeled $H_a$-$H_b$, Figure 4b) onto the neighboring hydride ($H_c$). Concomitant rotation of this new $\eta^2$-$H_c$-$H_b$ moiety then delivers $H_c$ back onto $H_a$ to complete the exchange. In **TS(4b-4b)**, the agostic interaction shortens significantly (Ru⋯$H_d$ = 1.91 Å; cf. 2.06 Å in **4b**), reflecting the lower trans influence of the $\eta^2\text{-}H_2$ moiety in comparison to a hydride. The overall barrier (relative to the lowest energy form **4c**) is 13.3 kcal/mol, consistent with rapid exchange on the NMR time scale.

The amine−borane complexes[32] $[Ru(IPr)_2(CO)(\kappa^2\text{-}H_2BH\cdot NMe_2H)H]BAr_4^F$ (**5**) and $[Ru(IPr)_2(CO)(\kappa^2\text{-}H_2BH\cdot NH_3)H]BAr_4^F$ (**6**) were prepared as alternative examples involving $\sigma$ E−H bond coordination to **2** (Scheme 4). **5** and **6** were identified in the first instance by the appearance of $^{11}B$ NMR signals at $\delta$ 4.5 and −2.4, respectively, characteristically downfield from those of the free substrates ($\delta$ −13.4, −21.6).[33,34] In the low-
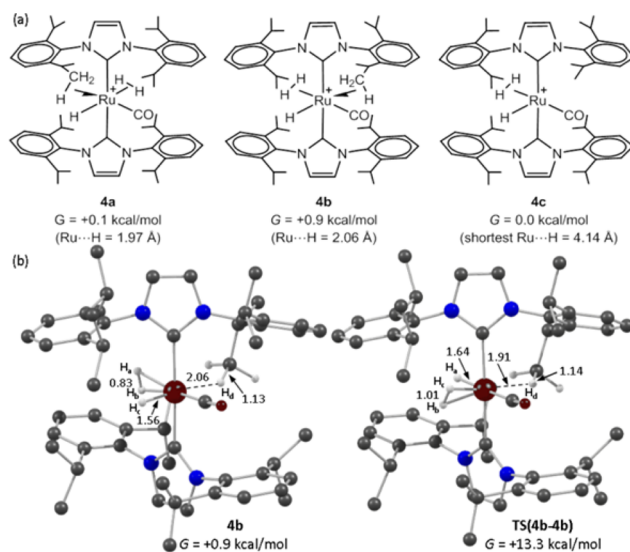


**Figure 4.** (a) Isomers of $[Ru(IPr)_2(CO)(\eta^2\text{-}H_2)H]^+$ (**4**), with the shortest agostic Ru⋯H contact indicated. (b) Computed structures of **4b** and Ru−H/$(\eta^2\text{-}H_2)$ exchange transition state **TS(4b-4b)** with selected distances in Å. Nonparticipating H atoms are omitted for clarity. All free energies (kcal/mol) are at the BP86-D3($CH_2Cl_2$) level and are quoted relative to **4c**, set to 0.0 kcal/mol.

frequency region of the $^1H$ NMR spectra, sharp hydride signals (**5**, $\delta$ −15.61; **6**, $\delta$ −15.86) were present in a 1:3 ratio with very broad B−H resonances (**5**, $\delta$ −2.3; **6**, $\delta$ −2.1). Upon cooling to 190 K, exchange of the bound and terminal B−H groups was frozen out to give two distinct, single-integral Ru−H−B singlets (**5**, $\delta$ −5.83, −3.94; **6**, $\delta$ −5.63, −4.13), which sharpened upon $^{11}B$ decoupling. In the case of **5**, $^1H\{^{11}B\}$ NOESY studies showed that the remaining, unbound B−H signal was hidden underneath resonances from the IPr groups. The X-ray structures of both **5** and **6** (Figure 5) revealed distorted-octahedral geometries comprised of a trans arrangement of IPr ligands with the CO and hydride then mutually cis and, therefore, trans to the two metal-bound B−H groups of the amine−borane ligands. The Ru⋯B distances of 2.293(4) and 2.333(2) Å were similar to the values in the large number of known rhodium $\kappa^2$-bound derivatives (e.g., $[Rh(P^iBu_3)_2(\kappa^2\text{-}$
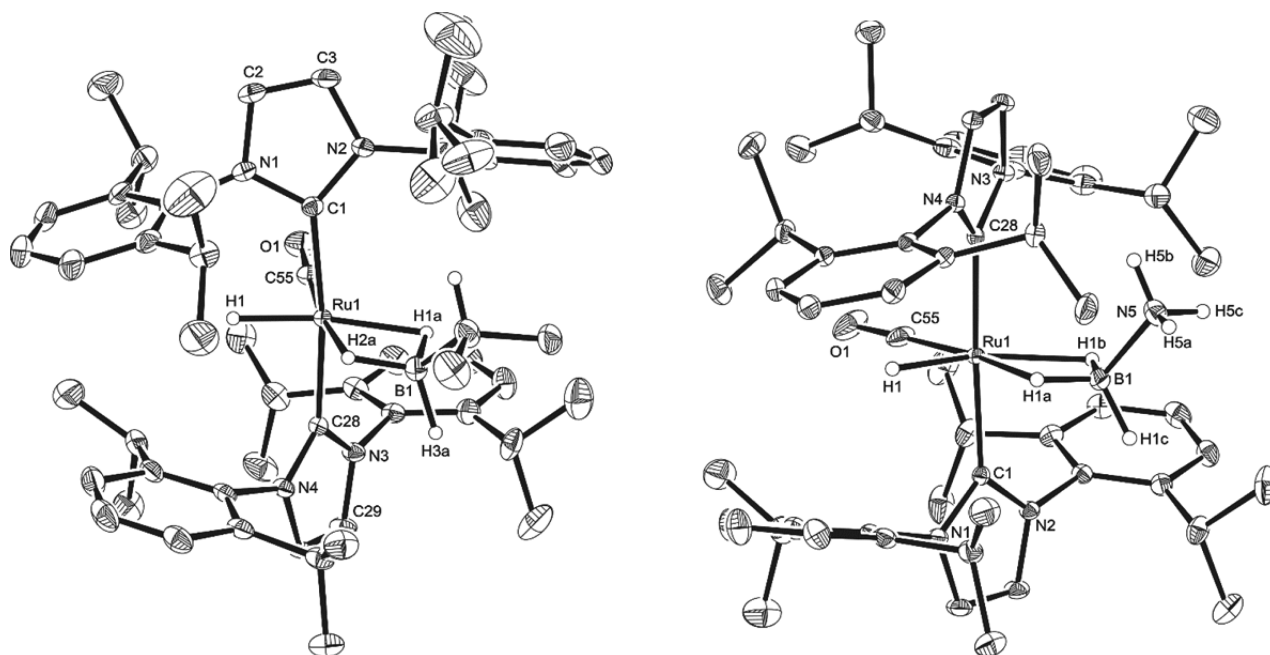
**Figure 5.** Molecular structure of the cations in (left) $[Ru(IPr)_2(CO)(\kappa^2\text{-}H_2BH\cdot NMe_2H)H]BAr_4^F$ (**5**) and (right) $[Ru(IPr)_2(CO)(\kappa^2\text{-}H_2BH\cdot NH_3)H]BAr_4^F$ (**6**). Ellipsoids are shown at the 30% probability level with all hydrogen atoms (except Ru–H and those on B or N) removed for clarity. Selected bond lengths (Å) and angles (deg) in **5**: Ru(1)–C(1) 2.136(3), Ru(1)–C(28) 2.107(3), Ru(1)–C(55) 1.805(4), Ru(1)–B(1) 2.293(4); C(1)–Ru(1)–C(28) 173.11(13), C(55)–Ru(1)–B(1) 142.06(16). Selected bond lengths (Å) and angles (deg) in **6**: Ru(1)–C(1) 2.1170(16), Ru(1)–C(28) 2.0950(16), Ru(1)–C(55) 1.813(2), Ru(1)–B(1) 2.333(2); C(1)–Ru(1)–C(28) 176.78(6), C(55)–Ru(1)–B(1) 162.34(10).

$H_2BH\cdot NMe_2H)H_2]^+$ (2.318(8) Å),[33,35] $[Rh(IMes)_2(\kappa^2\text{-}H_2BH\cdot N^tBuH_2)H_2]^+$ (2.305(4) Å)[36]) although (unsurprisingly) significantly shorter than those in the $\kappa^1$-bound ruthenium complexes $[Ru(xantphos)(PPh_3)(\kappa^1\text{-}HBH_2\cdot NH_3)H]^+$ (2.939(3) Å)[37] and $[Cp'Ru(PMe_3)_2(\kappa^1\text{-}HBH_2\cdot NMe_3)]^+$ (2.648(3) Å).[38]

The stability of **5** in solution proved to be solvent dependent. Thus, the complex decomposed in $CD_2Cl_2$ over ca. 6 h at room temperature but was stable for over 1 week in $C_6H_5F$. However, warming to 343 K in $C_6H_5F$ resulted in dehydrocoupling of the amine–borane ligand to afford $[Me_2N\text{-}BH_2]_2$ and the dihydrogen hydride complex **4**. Coordination of $H_2$ eliminated upon dehydrocoupling was also found[37] for $[Ru(xantphos)\text{-}(PPh_3)(\kappa^1\text{-}HBH_2\cdot N^tBuH_2)H]^+$ whereas, in contrast, amino–borane products of the type $[ML_2(\kappa^2\text{-}H_2B\text{-}NR_2)H_2]^+$ arise upon the dehydrocoupling of Rh and Ir amine–borane derivatives.[39] This difference is not simply due to Ru vs Rh/Ir, since $Ru(PCy_3)_2(\eta^2\text{-}H_2)H_2$ has also been shown to form the amino–borane product $Ru(PCy_3)_2(\kappa^2\text{-}H_2B\text{-}NR_2)H_2$ upon direct addition of $H_3B\cdot NR_2H$ (R = H, Me).[40] Extension of the bonding analysis performed by Alcaraz et al. on the isoelectronic and isostructural complexes $[M(PCy_3)_2(\kappa^2\text{-}H_2B\text{-}N^iPr_2)H_2]^{n+}$ (M = Ru, n = 0; M = Rh, Ir, n = 1) suggests that the inability of cationic **2** to coordinate an amino–borane ligand may be connected to poor overlap between the contracted metal d orbitals and empty BN $\pi^*$ orbital.[41]

In an attempt to promote $H_2B\text{-}NMe_2$ coordination, **5** was heated with an excess of $Me_3SiCH=CH_2$ as a hydrogen acceptor. This led, instead, to formation of the hydroboration product $Me_3SiCH_2CH_2BH_2NMe_2H$, which was identified by comparison of the $^{11}B$ NMR chemical shift to those of $RCH_2CH_2BH_2NMe_3$ (R = $^tBu$, $Me(CH_2)_3$).[42] The initial organometallic product of the reaction was **2**, implying that

alkene hydrogenation must occur as well as hydroboration. Continued heating led to the slow disappearance of the hydride signal for **2** (15 days at 323 K in $C_6H_5F$), alongside a change in color of the solution from orange to red. Spectroscopic identification of the product(s) proved to be a thankless task, due to extensive overlap of signals in both the methyl and methine regions of the proton NMR spectrum.

Fortuitous isolation of a very small number of diffraction-quality red-orange crystals proved possible. These were characterized by X-ray crystallography (Figure 6) as the C–H activated IPr complex $[Ru(IPr)(IPr)'(CO)]BAr_4^F$ (**7**). The sawhorse structure (C(1)–Ru(1)–C(29) 175.67(9)°; C(28)–Ru(1)–C(12) 96.40(12)°) shows an agostic interaction trans to the activated arm of the IPr ligand (Ru(1)···H(51C) 2.23(2) Å, Ru(1)···C(51) 3.163(3) Å, Ru(1)–H(51C)–C(51) 158(2)°). This was confirmed by a QTAIM calculation based on the heavy-atom positions of **7** that showed a Ru(1)···H51c bond path with $\rho(r)$ = 0.035 au (see Figure S19 in the Supporting Information). The metalated C–Ru distance of 2.071(2) Å is much shorter than those in either $[Ir(IPr)'(IPr)''H]^+$ (2.117(7) Å)[43] or $[Pt(IPr)(IPr)']^+$ (2.226(6) Å)[20], which to the best of our knowledge are the only other known examples of C–H activated IPr complexes.

**B–H Activation by 2.** The electrophilic nature of the Ru–H bond in **2** was demonstrated by the reaction with HBcat, which generated a rare example of a cationic boryl complex,[44] $[Ru(IPr)_2(CO)(Bcat)]BAr_4^F$ (**8**, Scheme 4). The formation of a boryl ligand was implied in the first instance by a signal at ca. $\delta$ 42 in the $^{11}B$ NMR spectrum, which is indicative of three-coordinate boron.[45] Free rotation about the Ru–B bond (on the basis of the appearance of two proton and three $^{13}C$ catechol signals) could be frozen out at 213 K, while lowering the temperature further (to 182 K) resolved the methine
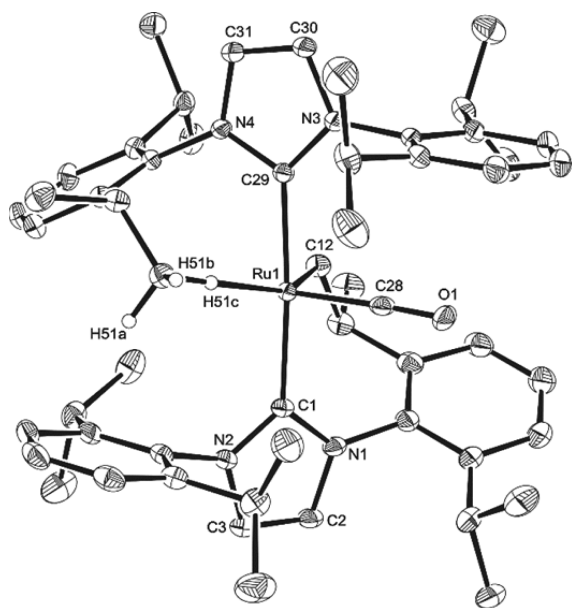
**Figure 6.** Molecular structure of the cation in [Ru(IPr)(IPr)′(CO)]-BAr$_4$$^F$ (**7**). Ellipsoids are shown at the 30% probability level with all hydrogen atoms (except those on the agostic methyl group) removed for clarity. Selected bond lengths (Å) and angles (deg): Ru(1)−C(1) 2.106(2), Ru(1)−C(29) 2.113(2), Ru(1)−C(28) 1.788(3), Ru(1)−C(12) 2.071(2); C(1)−Ru(1)−C(29) 175.67(9), C(12)−Ru(1)−C(28) 96.40(12).



**Figure 7.** Combined X-ray/neutron structure of the cation in [Ru(IPr)$_2$(CO)(Bcat)]BAr$_4$$^F$ (**8**). Ellipsoids are shown at the 30% probability level with all hydrogen atoms (except those on the agostic methyl group) removed for clarity. Selected bond lengths (Å) and angles (deg): Ru(1)−C(1) 2.141(4), Ru(1)−C(28) 2.138(4), Ru(1)−C(55) 1.834(5), Ru(1)−B(1) 2.030(4); C(1)−Ru(1)−C(28) 172.41(15), C(55)−Ru(1)−B(1) 84.1(2).
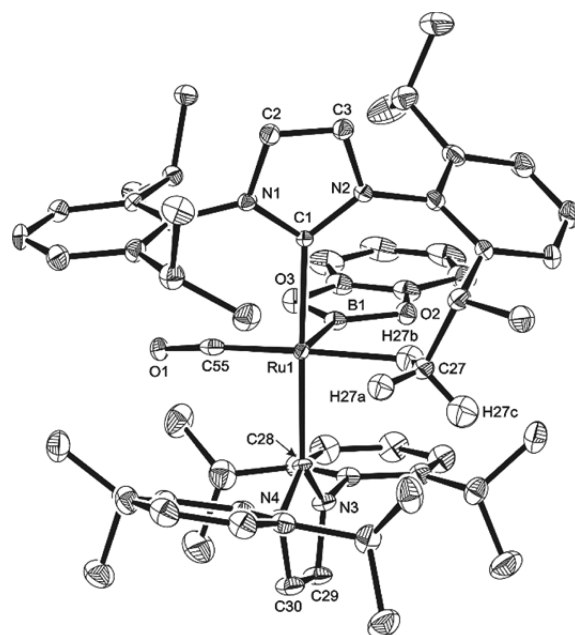
protons of the IPr ligands into eight multiplets, each of integral 1. The methyl resonances remained partially overlapping, although one doublet was shifted to low frequency to $\delta$ −0.34, consistent with agostic bonding.

This was investigated in the solid-state by a joint X-ray/neutron structure determination and QTAIM study. The former (Figure 7) revealed metrics similar to those seen in **2**, although with somewhat greater asymmetry in the closest Ru⋯H contacts (Ru(1)⋯C(27) 2.572(4) Å, Ru(1)⋯H(27b) 2.02(3) Å, Ru(1)⋯H(27a) 2.46(3) Å, Ru(1)⋯H(27b)−C(27) 109(2)°). The associated QTAIM molecular graph (Figure 8) this time indicates a single Ru⋯$\eta^2$-HC$^i$Pr $\xi$-agostic interaction, with no bond path evident between Ru1 and H27a and, hence, no RCP that would be indicative of the bifurcated Ru⋯$\eta^3$-H$_2$C form. The strong trans influence boryl ligand[46,47] occupied the apical site of the square-pyramidal structure, with an Ru−B distance (2.030(4) Å) much shorter than those found in other Ru or Os boryl complexes.[48] The catechol substituent provided the optimal motif for coordination to Ru, since no reaction at all was observed upon treatment of **2** with HBpin.

The reasons bifurcated Ru⋯$\eta^3$-H$_2$C structures are seen in **2a,b** while a Ru⋯$\eta^2$-HC interaction is preferred in **8** are presently not clear to us. Our DFT calculations on the isolated cations of **2a,b** indicate that structures with different (or indeed no) agostic interactions can be very close in energy. Moreover, a second-order perturbation analysis based on the computed natural bond orbitals (NBO) suggests that the overall strength of the agostic interaction does not reflect the binding mode. Thus, the total $\sigma$-donation from the C51−H51a and C51−H51b $\sigma$-BMOs is strongest in **2a** (21.2 kcal/mol), weakest in **2b** (12.4 kcal/mol), and intermediate from the C27−H27a and C27−H27b $\sigma$-BMOs in **8** (18.6 kcal/mol). See Figures S21 and S22 in the Supporting Information for full details.
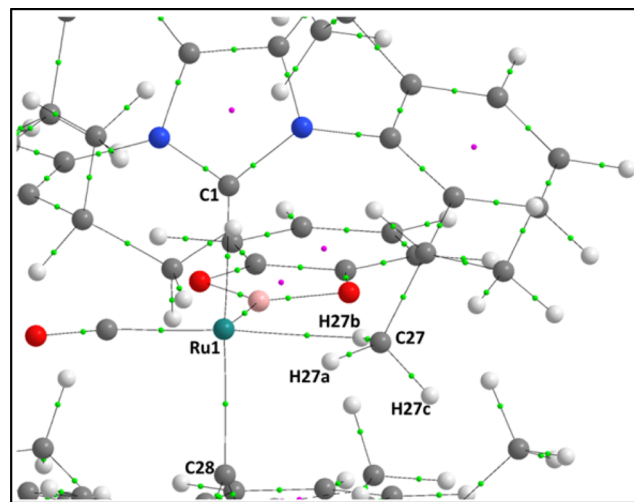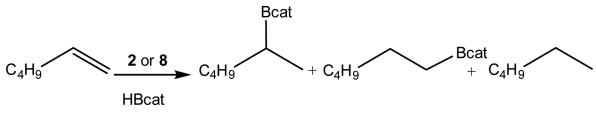


**Figure 8.** QTAIM molecular graph of **8** focusing on the Ru1⋯H27b interaction. Calculations were based on the experimental X-ray/neutron structure and used the BP86 functional. BCPs and RCPs are shown as green and magenta spheres, respectively. $\rho(r)$ for the Ru1⋯H51b BCP is 0.042 au. See the Supporting Information for full QTAIM metrics.

**Catalytic Hydroboration of Alkenes with 8.** Upon exposure of **8** to 1 atm of H$_2$, elimination of HBcat took place in the time of mixing with concomitant formation of the dihydrogen hydride complex **4**. The reversible coordination of the boryl ligand therefore prompted a preliminary study on the use of **8** as a precursor for catalytic alkene hydroboration. Rhodium, particularly with phosphine ligands,[49] is typically the element of choice for this transformation, with only a handful of reports detailing the activity of ruthenium complexes.[50]

Catalytic experiments with 1-hexene showed that **8** gave mainly the linear hydroboration product, with a small amount of hexane also generated through competitive alkene hydrogenation (Table 1). The hydride complex **2** gave an identical

## Table 1. Hydroboration of 1-Hexene[a]



|  |  | product ratio[b] | | |
|---|---|---|---|---|
| entry | Ru precursor | branched | linear | hexane |
| 1 | **8** | 14 | 80 | 6 |
| 2 | **2** | 18 | 76 | 6 |

[a]Conditions: 20 equiv of alkene, 40 equiv of HBcat in $C_6H_5F$, 298 K for 24 h, average of two runs. [b]Products and ratio determined by GC-MS and GC.

product composition, suggesting that it is converted to **8** under the catalytic conditions and that it is the boryl complex which then propagates the subsequent chemistry.[47]

## ■ SUMMARY AND CONCLUSIONS

The latent four-coordinate Ru(II) complex $[Ru(IPr)_2(CO)H]$-$BAr_4^F$ (**2**) has been prepared and shown by a combination of structural and computational methods to contain a bifurcated $Ru\cdots\eta^3$-$H_2C$ agostic interaction at one of the carbene $^iPr$ substituents. The agostic bonding appears to play a central role in allowing **2** to be isolated and structurally characterized, in contrast to the case for the non-agostic IMes derivative. In terms of reactivity, **2** behaves like a coordinatively unsaturated fragment, readily coordinating $H_2$, CO, and amine–boranes. Treatment with catecholborane highlights the electrophilic nature of the Ru–H bond, which results in the formation of the boryl derivative $[Ru(IPr)_2(CO)(Bcat)]BAr_4^F$, featuring a $Ru\cdots\eta^2$-HC interaction. This mode of reactivity, whereby substrates E–H (E = B, H) can add over the Ru–H bond, appears to be especially promising as a route to new Ru–E-containing products and is something we will report more on in due course.

## ■ EXPERIMENTAL SECTION

All manipulations were carried out using standard Schlenk, high-vacuum, and glovebox techniques using dried and degassed solvents, unless otherwise stated. NMR spectra were recorded on Bruker Avance 400 and 500 MHz NMR spectrometers and referenced to residual solvent signals for $^1H$ and $^{13}C$ spectra for $C_6D_6$ ($\delta$ 7.15, 128.0) and $CD_2Cl_2$ ($\delta$ 5.32, 54.0). Unlocked samples in fluorobenzene were referenced to the center of the downfield multiplet at $\delta$ 7.11. $^{11}B$ spectra were referenced externally to $BF_3\cdot OEt_2$ at $\delta$ 0.0. All complexes exhibited a singlet at $\delta$ −6.6 for the $BAr_4^F$ anion. IR spectra were recorded on a Nicolet Nexus spectrometer. Elemental analyses were performed by Elemental Microanalysis Ltd., Okehampton, Devon, U.K. GC-MS data were collected on an Agilent Technologies 5975C using an HP-5 column (GC data were collected on the same type of column). $Ru(IPr)_2(CO)HCl$ was prepared according to the literature.[19]

**$[Ru(IPr)_2(CO)H]BAr_4^F$ (2).** A $C_6H_5F$ (8 mL) solution of $Ru(IPr)_2(CO)HCl$ (0.21 g, 0.21 mmol) was added to a slurry of $NaBAr_4^F$ (0.192 g, 0.22 mmol) in $C_6H_5F$ (2 mL), and the suspension was stirred for 12 h. After filtration, the reaction mixture was concentrated to ca. 3 mL and layered with hexane to afford dark orange crystals of **2**, which were manually separated by hand from colorless crystals of residual $NaBAr_4^F$. Yield: 0.290 g (80%). $^1H$ NMR (500 MHz, $CD_2Cl_2$,

298 K): $\delta$ 7.74 (s, 8H, o-Ar-H), 7.58 (s, 4H, p-Ar-H), 7.45 (t, $^3J_{HH}$ = 7.7 Hz, 4H, p-Ar-H), 7.18−7.21 (overlapping d, 8H, m-Ar-H), 7.06 (s, 4H, NCH), 2.39 (sept, $^3J_{HH}$ = 7.0 Hz, 4H, CH(CH₃)₂), 2.32 (sept, $^3J_{HH}$ = 6.8 Hz, 4H, CH(CH₃)₂), 1.09 (d, $^3J_{HH}$ = 6.8 Hz, 12H, CH(CH₃)₂), 1.05 (d, $^3J_{HH}$ = 7.0 Hz, 12H, CH(CH₃)₂), 0.82 (d, $^3J_{HH}$ = 6.8 Hz, 12H, CH(CH₃)₂), 0.73 (d, $^3J_{HH}$ = 7.0 Hz, 12H, CH(CH₃)₂), −23.69 (s, 1H, Ru-H). $^{13}C\{^1H\}$ NMR (126 MHz, $CD_2Cl_2$, 298 K): $\delta$ 200.2 (s, Ru-CO), 185.4 (s, Ru-$C_{NHC}$), 162.2 (q, $^1J_{CB}$ = 50 Hz, i-ArC), 145.8 (s, o-ArC), 145.7 (s, o-ArC), 135.3 (s, o-ArC), 135.2 (s, NArC), 131.1 (s, p-ArC), 129.4 (qq, $^2J_{CF}$ = 32.2 Hz, $^4J_{CF}$ = 3.1 Hz), m-ArC), 125.8 (s, NCH), 125.1 (q, $^1J_{CF}$ = 270 Hz, $CF_3$), 125.0 (s, m-ArC), 124.7 (s, m-ArC), 117.9 (sept, $^3J_{CF}$ = 4 Hz, p-ArC), 29.2 (s, CH(CH₃)₂), 29.2 (s, CH(CH₃)₂), 24.6 (s, CH(CH₃)₂), 24.4 (s, CH(CH₃)₂), 23.8 (s, CH(CH₃)₂), 22.3 (s, CH(CH₃)₂). IR ($CH_2Cl_2$, cm⁻¹): 1964 ($\nu_{CO}$). Anal. Calcd for $C_{87}H_{85}BN_4OF_{24}Ru$: C, 59.02; H, 4.84; N, 3.16. Found: C, 58.91; H, 5.00; N, 3.29.

**$[Ru(IPr)_2(CO)_3H]BAr_4^F$ (3).** A J. Young resealable NMR tube was charged with a solution of **2** (0.043 g, 0.025 mmol) in $C_6H_5F$ (0.5 mL), degassed via three freeze−pump−thaw cycles, and exposed to 1 atm of CO. After 3 h, the pale yellow solution was layered with hexane to afford pale yellow crystals of **3**. Yield: 0.016 g (36%). $^1H$ NMR (500 MHz, $CD_2Cl_2$, 298 K): $\delta$ 7.73 (s, 8H, o-ArH), 7.56 (s, 4H, p-ArH), 7.51 (t, $^3J_{HH}$ = 8.1 Hz, 4H, p-ArH), 7.28 (d, $^3J_{HH}$ = 8.1 Hz, 8H, m-ArH), 7.16 (s, 4H, NCH), 2.21 (sept, $^3J_{HH}$ = 7.0 Hz, 8H, CH(CH₃)₂), 1.09 (d, $^3J_{HH}$ = 7.0 Hz, 24H, CH(CH₃)₂), 1.01 (d, $^3J_{HH}$ = 7.0 Hz, 24H, CH(CH₃)₂), −6.81 (s, 1H, RuH). $^{13}C\{^1H\}$ NMR (126 MHz, $CD_2Cl_2$, 298 K): $\delta$ 193.1 (s, Ru-CO), 189.6 (s, Ru-CO), 173.1 (s, Ru-$C_{NHC}$), 162.1 (q, $^1J_{CB}$ = 51 Hz, i-ArC), 146.4 (s, o-ArC), 136.6 (s, NArC), 135.2 (s, o-ArC), 132.0 (s, p-ArC), 129.2 (qq, $^2J_{CF}$ = 32 Hz, $^4J_{CF}$ = 3 Hz, m-ArC), 126.8 (s, NCH), 125.1 (s, m-ArC), 125.0 (q, $^1J_{CF}$ = 271.1 Hz, $CF_3$), 117.8 (m, p-ArC), 29.1 (s, CH(CH₃)₂), 26.3 (s, CH(CH₃)₂), 22.6 (s, CH(CH₃)₂). IR (KBr, cm⁻¹): 2040 ($\nu_{CO}$), 2025 ($\nu_{CO}$). Anal. Calcd for $C_{87}^{13}C_2H_{85}BN_4O_3F_{24}Ru$: C, 58.56; H, 4.69; N, 3.06. Found: C, 58.39; H, 4.60; N, 3.00.

**$[Ru(IPr)_2(CO)(\eta^2-H_2)H]BAr_4^F$ (4).** A J. Young resealable NMR tube was charged with a solution of **2** (0.010 g, 0.005 mmol) in $CD_2Cl_2$ (0.5 mL), degassed via three freeze−pump−thaw cycles, and exposed to 1 atm of $H_2$. After it was shaken, the tube was placed into the NMR spectrometer for characterization. $^1H$ NMR (400 MHz, $CD_2Cl_2$, 182 K): $\delta$ 7.72 (s, 8H, o-ArH), 7.53 (s, 4H, p-ArH), 7.44 (t, $^3J_{HH}$ = 7.5 Hz, 4H, p-ArH), 7.14 (d, $^3J_{HH}$ = 7.5 Hz 8H, m-ArH), 7.11 (s, 4H, NCH), 1.95 (m, 8H, CH(CH₃)₂), 0.89 (d, $^3J_{HH}$ = 5.4 Hz, 24H, CH(CH₃)₂), 0.82 (d, $^3J_{HH}$ = 5.4 Hz, 24H, CH(CH₃)₂), −4.95 (br s, 3H, RuH + Ru($\eta^2$-$H_2$)).

**$[Ru(IPr)_2(CO)(\kappa^2-H_2BH\cdot NMe_2H)H]BAr_4^F$ (5).** $H_3B\cdot NMe_2H$ (6 $\mu$L of 1.7 M solution in $C_6H_5F$, 0.01 mmol) was added to a solution of **2** (0.019 g, 0.01 mmol) in $C_6H_5F$ (0.5 mL). After 2 h, the solvent was removed in vacuo, and the residue was washed with hexane (3 × 0.4 mL) and then dried under vacuum. Layering the residue in fluorobenzene/hexane afforded pale yellow crystals of **5**. Yield: 0.017 g (78%). $^1H$ NMR (400 MHz, $CD_2Cl_2$, 298 K): $\delta$ 7.74 (s, 8H, o-ArH), 7.57 (s, 4H, p-ArH), 7.48 (t, $^3J_{HH}$ = 7.8 Hz, 4H, ArH), 7.23 (d, $^3J_{HH}$ = 7.8 Hz, 4H, ArH), 7.20 (d, $^3J_{HH}$ = 7.8 Hz, 4H, ArH), 7.00 (s, 4H, NCH), 2.75 (br s, 5H, NH + CH(CH₃)₂), 2.50 (br s, 4H, CH(CH₃)₂), 2.03/2.02 (s, 6H, N(CH₃)₂), 1.05 (d, $^3J_{HH}$ = 6.2 Hz, 24H, CH(CH₃)₂), 0.92 (d, $^3J_{HH}$ = 6.7 Hz, 24H, CH(CH₃)₂), −2.23 (br s, 3H, RuHB), −15.72 (s, 1H, RuH). $^1H$ NMR (500 MHz, $C_6H_5F$, 298 K): $\delta$ 8.37 (s, 8H, o-ArH), 7.68 (s, 4H, p-ArH), 2.81 (br s, 4H, CH(CH₃)₂), 2.68 (s, 1H, NH), 2.53 (br s, 4H, CH(CH₃)₂), 1.86 (s, 6H, N(CH₃)₂), 1.04 (d, $^3J_{HH}$ = 5.8 Hz, 12H, CH(CH₃)₂), 0.99 (d, $^3J_{HH}$ = 6.6 Hz, 12H, CH(CH₃)₂), 0.95 (br s, 12H, CH(CH₃)₂), 0.89 (d, $^3J_{HH}$ = 6.6 Hz, 12H, CH(CH₃)₂), −2.26 (br s, 3H, RuHB), −15.61 (s, 1H, RuH). Selected low temperature $^1H\{^{11}B\}$ NMR (400 MHz, $CD_2Cl_2$, 190 K): $\delta$ −3.94 (s, 1H, RuHB), −5.83 (s, 1H, RuHB), −15.33 (s, 1H, RuH). $^{11}B$ NMR (161 MHz, $C_6H_5F$, 298 K): $\delta$ 4.5 (br s, RuHB). IR (KBr, cm⁻¹): 1991 ($\nu_{RuH}$), 1953 ($\nu_{CO}$). Anal. Calcd for $C_{89}H_{95}B_2N_5OF_{24}Ru$: C, 58.42; H, 5.23; N, 3.83. Found: C, 58.35; H, 5.02; N, 3.87.

**$[Ru(IPr)_2(CO)(\kappa^2-H_2BH\cdot NH_3)H]BAr_4^F$ (6).** $H_3B\cdot NH_3$ (0.0004 g, 0.01 mmol) was added to a solution of **2** (0.021 g, 0.01 mmol) in

$C_6H_5F$ (0.5 mL). After 2 h, the solvent was removed in vacuo and the residue was washed with hexane (3 × 0.4 mL) and dried under vacuum. Recrystallization from fluorobenzene/hexane gave pale yellow crystals of **6**. Yield: 0.013 g (61%). ¹H NMR (500 MHz, $CD_2Cl_2$, 298 K): δ 7.73 (s, 8H, *o*-Ar*H*), 7.57 (s, 4H, *p*-Ar*H*), 7.46 (t, $^3J_{HH}$ = 7.7 Hz, 4H, Ar*H*), 7.20 (d, $^3J_{HH}$ = 7.8 Hz, 4H, Ar*H*), 7.18 (d, $^3J_{HH}$ = 8.0 Hz, 4H, Ar*H*), 6.99 (s, 4H, NC*H*), 2.89 (br s, 3H, N*H₃*), 2.56 (sept, $^3J_{HH}$ = 6.6 Hz, 4H, C*H*(CH₃)₂), 2.47 (sept, $^3J_{HH}$ = 7.0 Hz, 4H, C*H*(CH₃)₂), 1.03 (d, $^3J_{HH}$ = 7.0 Hz, 12H, CH(C*H₃*)₂), 1.00 (d, $^3J_{HH}$ = 6.6 Hz, 12H, CH(C*H₃*)₂), 0.93 (d, $^3J_{HH}$ = 7.0 Hz, 12H, CH(C*H₃*)₂), 0.88 (d, $^3J_{HH}$ = 6.6 Hz, 12H, CH(C*H₃*)₂), −2.15 (br s, 3H, Ru*H*B), −15.86 (s, 1H, Ru*H*). Selected low-temperature ¹H{¹¹B} NMR (400 MHz, $CD_2Cl_2$, 190 K): δ −4.13 (s, 1H, Ru*H*B), −5.63 (s, 1H, Ru*H*B), −14.95 (s, Ru*H*). ¹H NMR (500 MHz, $C_6H_5F$, 298 K): δ 8.36 (s, 8H, *o*-Ar*H*), 7.67 (s, 4H, *p*-Ar*H*), 2.88 (br s, 3H NH₃), 2.67 (sept, $^3J_{HH}$ = 6.9 Hz, 4H, CH(CH₃)₂), 2.55 (sept, $^3J_{HH}$ = 7.0 Hz, 4H, CH(CH₃)₂), 1.03 (d, $^3J_{HH}$ = 6.9 Hz, 12H, CH(C*H₃*)₂), 0.98 (d, $^3J_{HH}$ = 6.9 Hz, 12H, CH(C*H₃*)₂), 0.94 (d, $^3J_{HH}$ = 6.9 Hz, 12H, CH(C*H₃*)₂), 0.90 (d, $^3J_{HH}$ = 6.9 Hz, 12H, CH(C*H₃*)₂), −2.05 (br s, 3H, Ru*H*B), −15.88 (s, 1H, Ru*H*). ¹¹B NMR (161 MHz, $CD_2Cl_2$, 298 K): δ −2.4 (br s, Ru*H*B). IR (KBr, cm⁻¹): 1948 ($\nu_{CO}$). Anal. Calcd for $C_{87}H_{90}N_5B_2N_5OF_{24}Ru·C_6H_5F$: C, 58.90; H, 5.10; N, 3.69. Found: C, 58.35; H, 5.02; N, 3.87.

**[Ru(IPr)₂(CO)(Bcat)]BAr₄$^F$ (8).** HBcat (0.003 g, 0.025 mmol) was added to a solution of **2** (0.041 g, 0.023 mmol) in $C_6H_5F$ (0.5 mL), and the reaction mixture was allowed to stand for 1 h. The solvent was removed under vacuum to yield a pale brown solid, which was washed with hexane (3 × 0.8 mL) and then redissolved in fluorobenzene/hexane to afford **8** as pale yellow crystals. Yield: 0.034 g (78%). ¹H NMR (500 MHz, $CD_2Cl_2$, 298 K): δ 7.73 (s, 8H, *o*-Ar*H*), 7.57 (s, 4H, *p*-Ar*H*), 7.27 (m, 4H, Ar*H*), 7.21 (m, 4H, Ar*H*), 7.02 (d, $^3J_{HH}$ = 7.4 Hz, 4H, Ar*H*), 6.97 (s, 4H, NC*H*), 6.72 (dd, $^3J_{HH}$ = 5.4 Hz, $^3J_{HH}$ = 3.6 Hz, 2H, Ar*H*), 6.35 (dd, $^3J_{HH}$ = 5.4 Hz, $^3J_{HH}$ = 3.6 Hz, Ar*H*), 2.48 (sept, $^3J_{HH}$ = 6.8 Hz, 4H, C*H*(CH₃)₂), 2.31 (sept, $^3J_{HH}$ = 6.8 Hz, 4H, C*H*(CH₃)₂), 1.06 (d, $^3J_{HH}$ = 6.8 Hz, 24H, CH(C*H₃*)₂), 0.88 (d, $^3J_{HH}$ = 6.8 Hz, 12H, CH(C*H₃*)₂), 0.75 (d, $^3J_{HH}$ = 6.8 Hz, 12H, CH(C*H₃*)₂). Selected low-temperature ¹H NMR (400 MHz, $CD_2Cl_2$, 182 K): δ 2.70 (sept, $^3J_{HH}$ = 5.1 Hz, 1H, C*H*(CH₃)₂), 2.50 (sept, $^3J_{HH}$ = 6.7 Hz, 1H, C*H*(CH₃)₂), 2.42 (sept, $^3J_{HH}$ = 6.2 Hz, 1H, C*H*(CH₃)₂), 2.35 (sept, $^3J_{HH}$ = 6.0 Hz, 1H, C*H*(CH₃)₂), 2.23 (m, 1H, C*H*(CH₃)₂), 2.13 (sept, $^3J_{HH}$ = 5.7 Hz, 1H, C*H*(CH₃)₂), 1.97 (sept, $^3J_{HH}$ = 5.8 Hz, 1H, C*H*(CH₃)₂), 1.68 (sept, $^3J_{HH}$ = 6.5 Hz, 1H, C*H*(CH₃)₂), 1.38 (br s, 3H, CH(C*H₃*)₂), 1.26 (br s, 6H, CH(C*H₃*)₂), 1.20 (br s, 3H, CH(C*H₃*)₂), 1.15 (br s, 3H, CH(C*H₃*)₂), 1.10 (br s, 3H, CH(C*H₃*)₂), 0.97 (br s, 3H, CH(C*H₃*)₂), 0.88 (br s, 3H, CH(C*H₃*)₂), 0.81 (d, $^3J_{HH}$ = 6.0 Hz, 3H, CH(C*H₃*)₂), 0.76 (d, $^3J_{HH}$ = 5.1 Hz, 6H, CH(C*H₃*)₂), 0.62 (d, $^3J_{HH}$ = 5.7 Hz, 3H, CH(C*H₃*)₂), 0.49 (d, $^3J_{HH}$ = 6.5 Hz, 3H, CH(C*H₃*)₂), 0.32 (br s, 6H, CH(C*H₃*)₂), −0.34 (d, $^3J_{HH}$ = 6.0 Hz, 3H, CH(C*H₃*)₂). ¹³C{¹H} NMR (101 MHz, $CD_2Cl_2$, 298 K): δ 199.4 (s, Ru-CO), 182.2 (s, Ru-$C_{NHC}$), 162.2 (q, $^1J_{CB}$ = 50 Hz, *i*-Ar*C*), 149.5 (s, O*C*), 145.2 (s, *o*-Ar*C*), 135.3 (s, NAr*C*), 135.2 (s, *o*-Ar*C*), 130.8 (s, *p*-Ar*C*), 129.0 (qq, $^2J_{CF}$ = 32 Hz, $^4J_{CF}$ = 3 Hz, *m*-Ar*C*), 126.9 (s, NC*H*), 125.8 (s, *m*-Ar*C*), 125.0 (q, $^1J_{CF}$ = 271 Hz, *C*F₃), 124.6 (s, *m*-Ar*C*), 120.9 (s, Ar*C*), 117.8 (sept, $^3J_{CF}$ = 4 Hz, *p*-Ar*C*), 112.1 (s, Ar*C*), 29.8 (s, CH(CH₃)₂), 29.1 (s, CH(CH₃)₂), 25.1 (s, CH(CH₃)₂), 24.8 (s, CH(CH₃)₂), 22.4 (s, CH(CH₃)₂), 21.2 (s, CH(CH₃)₂). ¹¹B NMR (161 MHz, $CD_2Cl_2$, 298 K): δ 41.6 (br s, Ru*B*). IR ($CD_2Cl_2$, cm⁻¹): 1981 ($\nu_{CO}$). Anal. Calcd for $C_{93}H_{88}B_2N_4O_3F_{24}Ru$: C, 59.14; H, 4.70; N, 2.97. Found: C, 59.01; H, 4.55; N, 3.08.

**Catalytic Hydroboration.** To a solution of **2** (0.004 g, 0.0022 mmol) in $C_6H_5F$ (0.5 mL) in a vial in the glovebox were added 1-hexene (0.004 g, 0.0440 mmol) and HBcat (0.011 g, 0.088 mmol), and the reaction mixture was stirred for 24 h. At this time, ¹H NMR spectroscopy showed no resonances attributable to any remaining 1-hexene. The composition of the reaction mixture was analyzed by GC-MS; assignment of the linear product (and, by default, therefore the branched product) was made by comparison of retention time to a sample comprising ca. 99% of linear isomer prepared via the hydroboration of 1-hexene using Rh(PPh₃)₃Cl.[51]

**Crystallography.** Data for the combined X-ray (Mo Kα) and neutron refinement of **2** were collected using a Nonius kappaCCD

diffractometer and on the SXD time-of-flight Laue single-crystal diffractometer instrument at the ISIS spallation neutron source,[52] respectively. The neutron experiment for **2** was carried out using two single crystals that were mounted in random orientations relative to each other inside a sealed vanadium container filled with argon gas.[53] The vanadium can was loaded into a top-loading closed-cycle refrigerator, and data were collected at three different orientations. A Nonius kappaCCD instrument was also employed for the data collection of **3**, while those for **5** and **6** were effected using an Agilent Xcalibur (Mo Kα) diffractometer and that for **7** was completed using an Agilent SuperNova (Cu Kα) diffractometer. The structure of **8** was refined using a combination of X-ray data garnered using Cu Kα radiation and an Agilent SuperNova diffractometer plus neutron data on the SXD instrument at ISIS. In the latter experiment, one crystal was sealed inside a vanadium container under argon and placed into a top-loading closed-cycle refrigerator with data collected at five different orientations. All diffraction measurements were made at 150 K.

All of the X-ray refinements were carried out using SHELXL.[54] With the exception of **6**, the asymmetric unit in all structures comprises one cation and one BAr₄$^F$ anion. Hydrides, where present, were located and refined at a distance of 1.6 Å from the metal center in the case of the X-ray-only refinements for **3**, **5**, and **6**. Disorder of the fluorine atoms in some of the anion CF₃ groups was not uncommon. In such instances, C−F and F···F distance restraints were included, and if merited, ADP restraints were added for affected fractional occupancy fluorine atoms. Convergence was reasonably straightforward with the exception of the pertinent details, many of which pertain to disorder, that follow.

The model in **2**, which was solved and refined using X-ray data, revealed that two of the isopropyl groups in the cation were disordered, with the positions of C54/C55 and the carbon atoms attached to C41 (C42/C43) each being split over two sites in a 55:45 ratio. Some C−C distance restraints were employed to help convergence to a chemically sensible finale. The hydrogen atoms attached to C51 were located and freely refined, subject to being located 0.98 Å from the parent atom. The hydride ligand was seen to be disordered over two trans sites (55:45 ratio), and each fraction was refined at a distance of 1.6 Å from Ru1. In the BAr₄$^F$ anion, the fluorines attached to C79, C86, and C87 each exhibited disorder over two sites in respective ratios of 70:30, 60:40, and 50:50. The arising converged X-ray model was used as the basis for the results presented here, which were obtained using Jana2006[55] and a combination of X-ray and neutron data. With the exception of H51A, H51B, and H51C, the disordered hydride (H1/H1A) hydrogens were initially refined in four groups: namely, those confined to the anion and, in the cation, primary hydrogens, tertiary hydrogens, and aromatic hydrogens. The arising refined C−H distances were used as the basis for the rigid groups with which these noncontentious hydrogens were ultimately included. The disordered hydride was modeled subject to both components being equidistant from the ruthenium center. The agostic hydrogens attached to C51 were refined freely. All hydrogen atoms were treated isotropically. Disordered fluorine atoms were refined with ADP restraints and with restrained C−F and F···F distances of 1.330(5) and 2.14(3) Å, respectively.

Halide disorder was seen to bedevil many of the CF₃ groups within the anion in **3**. In particular, the fluorine atoms attached to C64, C65, C72, C80, C81, and C89 exhibited respective disorders of 65:35, 50:50, 70:30, 50:50, 80:20, and 55:45. C−F distances were restrained to being similar within each affected functionality. The isopropyl carbons, C23/C24, belonging to the cation in **6** were modeled as being disordered over two sites in a 55:45 ratio. The hydrogen atom attached to C22 was included at a calculated position on the basis of the major fractional occupancy components of C23/C24. H5 (attached to N5) was located and refined, subject to being located at a distance of 0.98 Å from the parent atom. The hydrogen atoms attached to the boron center, B1, were located and refined without restraints. Disorder was also evident in some of the anion CF₃ groups. In particular, the fluorine atoms attached to C64, C72, and C73 were each modeled over two proximate sites in disorder ratios of 50:50, 60:40, and 60:40,

respectively. In **6**, the hydrogen atoms attached to B1 and N5 were readily located and freely refined, without any restraints. There may be some "wagging" disorder associated with the carbonyl ligand. However, efforts to model this did not improve the refinement; hence, these were abandoned. Only one CF$_3$ group in the anion was modeled for disorder, with the fluorines attached to C62 being treated as located across two sites in a 75:25 ratio. There was also one disordered molecule of fluorobenzene in the asymmetric unit of this structure. This was ultimately treated using PLATON SQUEEZE, as the solvent was disordered over two proximate sites and, in each of these, the fractional fluorine was additionally disordered.

The asymmetric unit in **7** comprises one cation, one anion, half of an ordered molecule of C$_6$H$_5$F, and a region of diffuse solvent. C88, C91, H91, and F26 in the ordered solvent moiety are coincident with a crystallographic 2-fold rotation axis which serves to generate the remainder of the molecule. The disordered region exhibited some evidence for the presence of one fluorobenzene molecule, but this was not accessible to any sensible model and hence was treated via PLATON SQUEEZE. On the basis of the results from this algorithm, the empirical formula (as presented herein) contains one additional formula unit of C$_6$H$_5$F, to account for the SQUEEZED solvent. The hydrogen atoms attached to C51 were located and refined at a distance of 0.98 Å from the parent atom and subjected to being equidistant from each other. In the anion, F16–F18 were refined as being disordered over two proximate sites in a 65:35 ratio.

As for **2**, the structure of **8** was solved to convergence using X-ray data and the arising model then used as the basis for a combined refinement[55] using both X-ray and neutron data. In the X-ray-only model, the hydrogens attached to C27 were located and refined at a distance of 0.98 Å from the parent atom and with a common $U_{iso}$ value. Additionally, the hydrogen atoms attached to C12 were included at calculated positions but, again, with a common $U_{iso}$ value. Two of the CF$_3$ groups in the anion were modeled for disorder (55:45 and 60:40 ratios for fluorine atoms attached to C69 and C76, respectively). The combined X-ray and neutron refinement for this structure, with particular emphasis on the treatment of noncontentious hydrogen atoms, was similar to the strategy adopted for **2**. Ultimately, in this instance, the hydrogens attached to C27 were refined without restraints.

Crystallographic data for compounds **2**, **3**, and **5–8** have been deposited with the Cambridge Crystallographic Data Centre as supplementary publication nos. CCDC 1435594–1435599. Copies of the data can be obtained free of charge on application to CCDC, 12 Union Road, Cambridge CB2 1EZ, U.K. (fax (+44) 1223 336033, e-mail deposit@ccdc.cam.ac.uk).

**Computational Details.** DFT calculations were run with Gaussian 03 (Revision D.01)[56] and Gaussian 09 (Revision D.01).[57] Ru centers were described with the Stuttgart RECPs and associated basis sets,[58] and 6-31G** basis sets were used for all other atoms.[59] Optimizations employed the BP86[60] functional, and all stationary points were fully characterized via analytical frequency calculations as either minima (all positive eigenvalues) or transition states (one negative eigenvalue). Exceptions were those structures used for the QTAIM and NBO studies, which were either based on the X-ray/neutron structures (**2a,b** and **8**) or the experimental heavy-atom positions with only the H atoms positions being optimized (**7**). **TS(4b-4b)** was also characterized via IRC calculations and subsequent geometry optimizations to confirm it linked to the expected minima. PCM corrections for the effects of fluorobenzene and CH$_2$Cl$_2$ solvent were computed as appropriate with Gaussian 09 and dispersion corrections applied using Grimme's D3 parameter set[61] using the BP86-optimized geometries. QTAIM studies employed the AIMALL program,[62] and NBO analyses were run with NBO version 5.9.[63]

## ASSOCIATED CONTENT

### $\mathbf{\circleds}$ Supporting Information

All data supporting this study are provided as Supporting Information accompanying this paper. The Supporting Information is available free of charge on the ACS Publications website at DOI: 10.1021/acs.organomet.6b00173.

Multinuclear NMR spectra of **2–6** and **8**, computational data including full QTAIM data for BCPs and RCPs associated with Ru···H agostic interactions, details of TDDFT calculations, optimized geometries and energies and geometries used in QTAIM calculations, and an NBO analysis of the agostic interactions in **2a,b** and **8** (PDF)

Cartesian coordinates of all calculated geometries (XYZ)

Crystallographic data for **2**, **3**, and **5–8** (CIF)

## AUTHOR INFORMATION

### Corresponding Authors
*S.A.M.: e-mail, s.a.macgregor@hw.ac.uk.
*M.F.M.: e-mail, M.F.Mahon@bath.ac.uk.
*H.A.S.: e-mail, hazel.sparkes@bristol.ac.uk.
*M.K.W.: e-mail, m.k.whittlesey@bath.ac.uk; tel, 44 1225 383748.

### Present Address
$^{\perp}$School of Chemistry, University of St Andrews, St Andrews, Fife KY16 9ST, U.K.

### Notes
The authors declare no competing financial interest.

## REFERENCES

(1) Chatt, J.; Davidson, J. M. *J. Chem. Soc.* **1965**, 843−855.

(2) (a) Ittel, S. D.; Tolman, C. A.; English, A. D.; Jesson, J. P. *J. Am. Chem. Soc.* **1976**, *98*, 6073−6075. (b) Ittel, S. D.; Tolman, C. A.; English, A. D.; Jesson, J. P. *J. Am. Chem. Soc.* **1978**, *100*, 7577−7585. (c) Tolman, C. A.; Ittel, S. D.; English, A. D.; Jesson, J. P. *J. Am. Chem. Soc.* **1979**, *101*, 1742−1751.

(3) (a) Hall, C.; Jones, W. D.; Mawby, R. J.; Osman, R.; Perutz, R. N.; Whittlesey, M. K. *J. Am. Chem. Soc.* **1992**, *114*, 7425−7435. (b) Osman, R.; Perutz, R. N.; Rooney, A. D.; Langley, A. J. *J. Phys. Chem.* **1994**, *98*, 3562−3563.

(4) (a) Ogasawara, M.; Macgregor, S. A.; Streib, W. E.; Folting, K.; Eisenstein, O.; Caulton, K. G. *J. Am. Chem. Soc.* **1995**, *117*, 8869−8870. (b) Ogasawara, M.; Macgregor, S. A.; Streib, W. E.; Folting, K.; Eisenstein, O.; Caulton, K. G. *J. Am. Chem. Soc.* **1996**, *118*, 10189−10199. See also: Ogasawara, M.; Huang, D.; Streib, W. E.; Huffman, J. C.; Gallego-Planas, N.; Maseras, F.; Eisenstein, O.; Caulton, K. G. *J. Am. Chem. Soc.* **1997**, *119*, 8642−8651.

(5) Flügel, R.; Windmüller, B.; Gevert, O.; Werner, H. *Chem. Ber.* **1996**, *129*, 1007−1013.

(6) (a) Watson, L. A.; Ozerov, O. V.; Pink, M.; Caulton, K. G. *J. Am. Chem. Soc.* **2003**, *125*, 8426−8427. (b) Ingleson, M. J.; Yang, X.; Pink, M.; Caulton, K. G. *J. Am. Chem. Soc.* **2005**, *127*, 10846−10847. (c) Walstrom, A.; Pink, M.; Caulton, K. G. *Inorg. Chem.* **2006**, *45*, 5617−5620.

(7) (a) Askevold, B.; Khusniyarov, M. M.; Herdtweck, E.; Meyer, K.; Schneider, S. *Angew. Chem., Int. Ed.* **2010**, *49*, 7566−7569. (b) Schneider, S.; Meiners, J.; Askevold, B. *Eur. J. Inorg. Chem.* **2012**, *2012*, 412−429. (c) Askevold, B.; Khusniyarov, M. M.; Kroener,

W.; Gieb, K.; Müller, P.; Herdtweck, E.; Heinemann, M.; Diefenbach, M.; Holthausen, M. C.; Vieru, V.; Chibotaru, L. F.; Schneider, S. *Chem. - Eur. J.* **2015**, *21*, 579−589.

(8) MacInnis, M. C.; McDonald, R.; Ferguson, M. J.; Tobisch, S.; Turculet, L. *J. Am. Chem. Soc.* **2011**, *133*, 13622−13633.

(9) Huang, D.; Streib, W. E.; Eisenstein, O.; Caulton, K. G. *Angew. Chem., Int. Ed. Engl.* **1997**, *36*, 2004−2006.

(10) Huang, D.; Streib, W. E.; Bollinger, J. C.; Caulton, K. G.; Winter, R. F.; Scheiring, T. *J. Am. Chem. Soc.* **1999**, *121*, 8087−8097.

(11) Huang, D.; Bollinger, J. C.; Streib, W. E.; Folting, K.; Young, V., Jr.; Eisenstein, O.; Caulton, K. G. *Organometallics* **2000**, *19*, 2281−2290.

(12) Baratta, W.; Herdtweck, E.; Rigo, P. *Angew. Chem., Int. Ed.* **1999**, *38*, 1629−1631.

(13) (a) Huang, D.; Folting, K.; Caulton, K. G. *J. Am. Chem. Soc.* **1999**, *121*, 10318−10322. (b) Huang, D.; Gérard, H.; Clot, E.; Young, V., Jr.; Streib, W. E.; Eisenstein, O.; Caulton, K. G. *Organometallics* **1999**, *18*, 5441−5443.

(14) Catalá, R.-M.; Cruz-Garritz, D.; Sosa, P.; Terreros, P.; Torrens, H.; Hills, A.; Hughes, D. L.; Richards, R. L. *J. Organomet. Chem.* **1989**, *359*, 219−232.

(15) For cases which seem to be devoid of such stabilization, see: (a) Sanford, M. S.; Henling, L. M.; Day, M. W.; Grubbs, R. H. *Angew. Chem., Int. Ed.* **2000**, *39*, 3451−3453. (b) Conrad, J. C.; Amoroso, D.; Czechura, P.; Yap, G. P. A.; Fogg, D. E. *Organometallics* **2003**, *22*, 3634−3636. (c) Romero, P. E.; Piers, W. E.; McDonald, R. *Angew. Chem., Int. Ed.* **2004**, *43*, 6161−6165. (d) Singh, A. K.; Levine, B. G.; Staples, R. J.; Odom, A. L. *Chem. Commun.* **2013**, *49*, 10799−10801.

(16) Baratta, W.; Mealli, C.; Herdtweck, E.; Ienco, A.; Mason, S. A.; Rigo, P. *J. Am. Chem. Soc.* **2004**, *126*, 5549−5562. For other non-Ru examples, see: (a) Crosby, S. H.; Clarkson, G. J.; Rourke, J. P. *J. Am. Chem. Soc.* **2009**, *131*, 14142−14143. (b) Cole, J. M.; Waddell, P. G.; Wheatley, A. E. H.; McIntyre, G. J.; Peel, A. J.; Tate, C. W.; Linton, D. J. *Organometallics* **2014**, *33*, 3919−3923.

(17) Lee, J. P.; Ke, Z.; Ramírez, M. A.; Gunnoe, T. B.; Cundari, T. R.; Boyle, P. D.; Petersen, J. L. *Organometallics* **2009**, *28*, 1758−1775.

(18) (a) Scott, N. M.; Dorta, R.; Stevens, E. D.; Correa, A.; Cavallo, L.; Nolan, S. P. *J. Am. Chem. Soc.* **2005**, *127*, 3516−3526. (b) Fantasia, S.; Egbert, J. D.; Jurčík, V.; Cazin, C. S. J; Jacobsen, H.; Cavallo, L.; Heinekey, D. M.; Nolan, S. P. *Angew. Chem., Int. Ed.* **2009**, *48*, 5182−5186.

(19) Chantler, V. L.; Chatwin, S. L.; Jazzar, R. F. R.; Mahon, M. F.; Saker, O.; Whittlesey, M. K. *Dalton Trans.* **2008**, 2603−2614.

(20) (a) Rivada-Wheelaghan, O.; Donnadieu, B.; Maya, C.; Conejero, S. *Chem. - Eur. J.* **2010**, *16*, 10323−10326. (b) Ortuño, M. A.; Conejero, S.; Lledós, A. *Beilstein J. Org. Chem.* **2013**, *9*, 1352−1382.

(21) Bader, R. F. W. *Atoms in Molecules - A Quantum Theory*; Oxford University Press: Oxford, U.K., 1990.

(22) Batool, M.; Martin, T. A.; Algarra, A.; George, M. W.; Macgregor, S. A.; Mahon, M. F.; Whittlesey, M. K. *Organometallics* **2012**, *31*, 4971−4979.

(23) See the Supporting Information for a figure showing the minor component.

(24) For recent discussions on the dynamics of agostically bound NHC ligands in low-coordinate cationic Pt(II) species, see: (a) Ortuño, M. A.; Vidossich, P.; Ujaque, G.; Conejero, S.; Lledós, A. *Dalton Trans.* **2013**, *42*, 12165−12172. (b) Ortuño, M. A.; Vidossich, P.; Conejero, S.; Lledós, A. *Angew. Chem., Int. Ed.* **2014**, *53*, 14158−14161.

(25) Huang, D.; Huffman, J. C.; Bollinger, J. C.; Eisenstein, O.; Caulton, K. G. *J. Am. Chem. Soc.* **1997**, *119*, 7398−7399.

(26) Tang, C. Y.; Thompson, A. L.; Aldridge, S. *J. Am. Chem. Soc.* **2010**, *132*, 10578−10591.

(27) As Gunnoe, Cundari, and co-workers employed the B3LYP functional in their work,[17] we repeated our calculations with the B3LYP-D3($C_6H_5F$)//B3LYP approach. This gave trends similar to the results in the main text, for $[Ru(IPr)_2(CO)(H)]^+$ (**2b** (0.0 kcal/mol) < **2a** (+0.3 kcal/mol) < **2c** (+3.3 kcal/mol)) and for $[Ru(IMes)_2(CO)$

(H)$]^+$ (**1c** (0.0 kcal/mol) < **1a** (+1.4 kcal/mol) < **1b** (+7.5 kcal/mol)). See the Supporting Information for full details.

(28) Siedle, A. R.; Newmark, R. A.; Gleason, W. B. *Inorg. Chem.* **1991**, *30*, 2005−2009.

(29) (a) Gusev, D. G.; Hübener, R.; Burger, P.; Orama, O.; Berke, H. *J. Am. Chem. Soc.* **1997**, *119*, 3716−3731. (b) Chen, Y.-Z.; Chan, W. C.; Lau, C. P.; Chu, H. S.; Lee, H. L.; Jia, G. *Organometallics* **1997**, *16*, 1241−1246. (c) Leñero, K. A.; Kranenburg, M.; Guari, Y.; Kamer, P. C. J.; van Leeuwen, P. W. N. M.; Sabo-Etienne, S.; Chaudret, B. *Inorg. Chem.* **2003**, *42*, 2859−2866. (d) Grellier, M.; Vendier, L.; Chaudret, B.; Albinati, A.; Rizzato, S.; Mason, S.; Sabo-Etienne, S. *J. Am. Chem. Soc.* **2005**, *127*, 17592−17593.

(30) For a review of M($\eta^2$-$H_2$)H species, see: Morris, R. H. *Coord. Chem. Rev.* **2008**, *252*, 2381−2394.

(31) This is in marked contrast to one of the few other known Ru-NHC dihydrogen complexes, $[Ru(NHC)_4(\eta^2$-$H_2)H]BAr_4^F$, in which both of the small N-alkyl-substituted NHCs 1,3-diethyl-4,5-dimethyl-limidazol-2-ylidene ($IEt_2Me_2$) and 1,2,4,5-tetramethylimidazol-2-ylidene ($IMe_4$) readily lose $H_2$ in solution upon freeze−pump−thaw degassing: Burling, S.; Häller, L. J. L.; Mas-Marzá, E.; Moreno, A.; Macgregor, S. A.; Mahon, M. F.; Pregosin, P. S.; Whittlesey, M. K. *Chem. - Eur. J.* **2009**, *15*, 10912−10923.

(32) Alcaraz, G.; Sabo-Etienne, S. *Angew. Chem., Int. Ed.* **2010**, *49*, 7170−7179.

(33) Douglas, T. M.; Chaplin, A. B.; Weller, A. S. *J. Am. Chem. Soc.* **2008**, *130*, 14432−14433.

(34) Jaska, C. A.; Temple, K.; Lough, A. J.; Manners, I. *J. Am. Chem. Soc.* **2003**, *125*, 9424−9434.

(35) Douglas, T. M.; Chaplin, A. B.; Weller, A. S.; Yang, X.; Hall, M. B. *J. Am. Chem. Soc.* **2009**, *131*, 15440−15456.

(36) Tang, C. Y.; Thompson, A. L.; Aldridge, S. *Angew. Chem., Int. Ed.* **2010**, *49*, 921−925.

(37) Ledger, A. E. W.; Ellul, C. E.; Mahon, M. F.; Williams, J. M. J.; Whittlesey, M. K. *Chem. - Eur. J.* **2011**, *17*, 8704−8713.

(38) Kawano, Y.; Hashiva, M.; Shimoi, M. *Organometallics* **2006**, *25*, 4420−4426.

(39) Stevens, C. J.; Dallanegra, R.; Chaplin, A. B.; Weller, A. S.; Macgregor, S. A.; Ward, B.; McKay, D.; Alcaraz, G.; Sabo-Etienne, S. *Chem. - Eur. J.* **2011**, *17*, 3011−3020.

(40) Alcaraz, G.; Vendier, L.; Clot, E.; Sabo-Etienne, S. *Angew. Chem., Int. Ed.* **2010**, *49*, 918−920.

(41) Alcaraz, G.; Chaplin, A. B.; Stevens, C. J.; Clot, E.; Vendier, L.; Weller, A. S.; Sabo-Etienne, S. *Organometallics* **2010**, *29*, 5591−5595.

(42) (a) Sewell, L. J.; Chaplin, A. B.; Weller, A. S. *Dalton Trans.* **2011**, *40*, 7499−7501. (b) Johnson, H. C.; Torry-Harris, R.; Ortega, L.; Theron, R.; McIndoe, J. S.; Weller, A. S. *Catal. Sci. Technol.* **2014**, *4*, 3486−3494.

(43) Tang, C. Y.; Smith, W.; Vidovic, D.; Thompson, A. L.; Chaplin, A. B.; Aldridge, S. *Organometallics* **2009**, *28*, 3059−3066.

(44) (a) Lu, Z.; Jun, C.-H.; de Gala, S. R.; Sigalas, M. P.; Eisenstein, O.; Crabtree, R. H. *Organometallics* **1995**, *14*, 1168−1175. (b) Rickard, C. E. F.; Roper, W. R.; Williamson, A.; Wright, L. J. *Organometallics* **1998**, *17*, 4869−4874. (c) Braunschweig, H.; Radacki, K.; Rais, D.; Scheschkewitz, D. *Angew. Chem., Int. Ed.* **2005**, *44*, 5651−5654. (d) Braunschweig, H.; Radacki, K.; Uttinger, K. *Chem. - Eur. J.* **2008**, *14*, 7858−7866. (e) Arnold, N.; Braunschweig, H.; Brenner, P.; Jimenez-Halla, J. O. C.; Kupfer, T.; Radacki, K. *Organometallics* **2012**, *31*, 1897−1907. (f) Buil, M. L.; Esteruelas, M. A.; Fernández, I.; Izquierdo, S.; Õnate, E. *Organometallics* **2013**, *32*, 2744−2752.

(45) (a) Irvine, G. J.; Lesley, M. J. G.; Marder, T. B.; Norman, N. C.; Rice, C. R.; Robins, E. G.; Roper, W. R.; Whittell, G. R.; Wright, L. J. *Chem. Rev.* **1998**, *98*, 2685−2722. (b) Kays, D. L.; Aldridge, S. *Struct. Bonding (Berlin)* **2008**, *130*, 29−122. (c) Aldridge, S.; Coombs, D. L. *Coord. Chem. Rev.* **2004**, *248*, 535−559.

(46) (a) Lam, K. C.; Lam, W. H.; Lin, Z.; Marder, T. B.; Norman, N. C. *Inorg. Chem.* **2004**, *43*, 2541−2547. (b) Zhu, J.; Lin, Z. Y.; Marder, T. B. *Inorg. Chem.* **2005**, *44*, 9384−9390.

(47) Dang, L.; Lin, Z.; Marder, T. B. *Chem. Commun.* **2009**, 3987−3995.

(48) (a) Rickard, C. E. F.; Roper, W. R.; Williamson, A.; Wright, L. J. *Organometallics* **2000**, *19*, 4344−4355. (b) Clark, G. R.; Irvine, G. J.; Roper, W. R.; Wright, L. J. *J. Organomet. Chem.* **2003**, *680*, 81−88. (c) Rickard, C. E. F.; Roper, W. R.; Williamson, A.; Wright, L. J. *J. Organomet. Chem.* **2004**, *689*, 1609−1616. (d) Rankin, M. A.; MacLean, D. F.; McDonald, R.; Ferguson, M. J.; Lumsden, M. D.; Stradiotto, M. *Organometallics* **2009**, *28*, 74−83. (e) Hill, A. F.; Lee, S. B.; Park, J.; Shang, R.; Willis, A. C. *Organometallics* **2010**, *29*, 5661−5669. (f) Koren-Selfridge, L.; Query, I. P.; Hanson, J. A.; Isley, N. A.; Guzei, I. A.; Clark, T. B. *Organometallics* **2010**, *29*, 3896−3900. (g) Hill, A. F.; McQueen, C. M. A. *Organometallics* **2014**, *33*, 1977−1985.

(49) Beletskaya, I.; Pelter, A. *Tetrahedron* **1997**, *53*, 4957−5026.

(50) (a) Burgess, K.; Jaspars, M. *Organometallics* **1993**, *12*, 4197−4200. (b) Caballero, A.; Sabo-Etienne, S. *Organometallics* **2007**, *26*, 1191−1195.

(51) Evans, D. A.; Fu, G. C.; Hoveyda, A. H. *J. Am. Chem. Soc.* **1992**, *114*, 6671−6679.

(52) Keen, D. A.; Gutmann, M. J.; Wilson, C. C. *J. Appl. Crystallogr.* **2006**, *39*, 714−722.

(53) Wilson, C. C. *J. Appl. Crystallogr.* **1997**, *30*, 184−189.

(54) Sheldrick, G. M. *Acta Crystallogr., Sect. A: Found. Crystallogr.* **1990**, *46*, 467−473. Sheldrick, G. M. *SHELXL-97, a computer program for crystal structure refinement*, University of Göttingen, Göttingen, Germany, 1997.

(55) Petricek, V.; Dusek, M.; Palatinus, L. *Z. Kristallogr. - Cryst. Mater.* **2014**, *229*, 345−352.

(56) Frisch, M. J.; Trucks, G. W.; Schlegel, H. B.; Scuseria, G. E.; Robb, M. A.; Cheeseman, J. R.; Montgomery, J. A.; Vreven, T.; Kudin, K. N.; Millam, J. M.; Iyengar, S. S.; Tomasi, J.; Barone, V.; Mennucci, B.; Cossi, M.; Scalmani, G.; Rega, N.; Petersson, G. A.; Nakatsuji, H.; Hada, M.; Ehara, M.; Toyota, K.; Fukuda, R.; Hasegawa, J.; Ishida, M.; Nakajima, T.; Honda, Y.; Kitao, O.; Nakai, H.; Klene, M.; Li, X.; Knox, J. E.; Hratchian, H. P.; Cross, J. B.; Bakken, V.; Adamo, C.; Jaramillo, J.; Gomperts, R.; Stratmann, R. E.; Yazyev, O.; Austin, A. J.; Cammi, R.; Pomelli, C.; Ochterski, J. W.; Ayala, P. Y.; Morokuma, K.; Voth, G. A.; Salvador, P.; Dannenberg, J. J.; Zakrzewski, V. G.; Dapprich, S.; Daniels, A. D.; Strain, M. C.; Farkas, O.; Malick, D. K.; Rabuck, A. D.; Raghavachari, K.; Foresman, J. B.; Ortiz, J. V.; Cui, Q.; Baboul, A. G.; Clifford, S.; Cioslowski, J.; Stefanov, B. B.; G. Liu, A. L.; Piskorz, P.; Komaromi, I.; Martin, R. L.; Fox, D. J.; Keith, T.; Al-Laham, M. A.; Peng, C. Y.; Nanayakkara, A.; Challacombe, M.; Gill, P. M. W.; Johnson, B.; Chen, W.; Wong, M. W.; Gonzalez, C.; Pople, J. A. *Gaussian 03, Revision D.01*, Gaussian, Inc., Wallingford, CT, 2004.

(57) Frisch, M. J.; Trucks, G. W.; Schlegel, H. B.; Scuseria, G. E.; Robb, M. A.; Cheeseman, J. R.; Scalmani, G.; Barone, V.; Mennucci, B.; Petersson, G. A.; Nakatsuji, H.; Caricato, M.; Li, X.; Hratchian, H. P.; Izmaylov, A. F.; Bloino, J.; Zheng, G.; Sonnenberg, J. L.; Hada, M.; Ehara, M.; Toyota, K.; Fukuda, R.; Hasegawa, J.; Ishida, M.; Nakajima, T.; Honda, Y.; Kitao, O.; Nakai, H.; Vreven, T.; Montgomery, J. A., Jr.; Peralta, J. E.; Ogliaro, F.; Bearpark, M.; Heyd, J. J.; Brothers, E.; Kudin, K. N.; Staroverov, V. N.; Kobayashi, R.; Normand, J.; Raghavachari, K.; Rendell, A.; Burant, J. C.; Iyengar, S. S.; Tomasi, J.; Cossi, M.; Rega, N.; Millam, J. M.; Klene, M.; Knox, J. E.; Cross, J. B.; Bakken, V.; Adamo, C.; Jaramillo, J.; Gomperts, R.; Stratmann, R. E.; Yazyev, O.; Austin, A. J.; Cammi, R.; Pomelli, C.; Ochterski, J. W.; Martin, R. L.; Morokuma, K.; Zakrzewski, V. G.; Voth, G. A.; Salvador, P.; Dannenberg, J. J.; Dapprich, S.; Daniels, A. D.; Farkas, O.; Foresman, J. B.; Ortiz, J. V.; Cioslowski, J.; Fox, D. J. *Gaussian 09, Revision D.01*, Gaussian, Inc., Wallingford, CT, 2013.

(58) Andrae, D.; Häußermann, U.; Dolg, M.; Stoll, H.; Preuß, H. *Theor. Chim. Acta* **1990**, *77*, 123−141.

(59) (a) Hehre, W. J.; Ditchfield, R.; Pople, J. A. *J. Chem. Phys.* **1972**, *56*, 2257−2261. (b) Hariharan, P. C.; Pople, J. A. *Theor. Chim. Acta* **1973**, *28*, 213−222.

(60) (a) Perdew, J. P. *Phys. Rev. B: Condens. Matter Mater. Phys.* **1986**, *33*, 8822−8824. (b) Becke, A. D. *Phys. Rev. A: At., Mol., Opt. Phys.* **1988**, *38*, 3098−3100.

(61) Grimme, S.; Antony, J.; Ehrlich, S.; Krieg, H. *J. Chem. Phys.* **2010**, *132*, 154104−1.

(62) Keith, T. A. *AIMAll (Version 13.02.26, Professional)*; TK Gristmill Software, Overland Park, KS, USA, 2015; aim.tkgristmill.com.

(63) Glendening, E. D.; Badenhoop, J. K.; Reed, A. E.; Carpenter, J. E.; Bohmann, J. A.; Morales, C. M.; Weinhold, F. *NBO 5.9*; Theoretical Chemistry Institute, University of Wisconsin, Madison, WI, 2009; http://www.chem.wisc.edu/~nbo5.